# Constraints on the genesis of the potassium-rich Italian volcanics from U/Th disequilibrium.

JOURNAL OF PETROLOGY | VOLUME 49 | NUMBER 2 | PAGES 195–223 | 2008 | doi:10.1093/petrology/egm076

# Constraints on the Genesis of Potassium-rich Italian Volcanic Rocks from U/Th Disequilibrium

**RICCARDO AVANZINELLI[1]*, TIM ELLIOTT[2], SIMONE TOMMASINI[1] AND SANDRO CONTICELLI[1,3]**

[1]DIPARTIMENTO DI SCIENZE DELLA TERRA, UNIVERSITÀ DEGLI STUDI DI FIRENZE, VIA GIORGIO LA PIRA, 4, I-50121, FIRENZE, ITALY

[2]BRISTOL ISOTOPE GROUP, DEPARTMENT OF EARTH SCIENCES, UNIVERSITY OF BRISTOL, WILLS MEMORIAL BUILDING, QUEEN'S ROAD, BRISTOL BS8 1RJ, UK

[3]ISTITUTO DI GEOSCIENZE E GEORISORSE, CNR, VIA GIORGIO LA PIRA, 4, I-50121, FIRENZE, ITALY

**RECEIVED NOVEMBER 8, 2006; ACCEPTED NOVEMBER 12, 2007**
**ADVANCE ACCESS PUBLICATION DECEMBER 12, 2007**

*We present new U-series isotope, $^{87}Sr/^{86}Sr$, $^{143}Nd/^{144}Nd$ and trace element data for a set of mafic, K-rich rocks from volcanoes in Central–Southern Italy. These shoshonitic to ultrapotassic lavas display strongly depleted high field strength element (HSFE) abundances with respect to other incompatible trace elements together with high but variable $^{87}Sr/^{86}Sr$ and low but variable $^{143}Nd/^{144}Nd$ values. Such characteristics are thought to be due to addition of subducted crust of variable amount and composition to their mantle sources prior to magma genesis. Rocks from the northernmost region (i.e. Tuscan Magmatic Province and Northern Roman Magmatic Province) display ($^{230}Th/^{238}U$) activity ratios close to radioactive equilibrium, suggesting that metasomatism of their sources occurred before 400 ka and recent melting took place at shallow depths, in the absence of garnet. A $^{238}U$ excess of up to 27% has been measured in rocks from the Neapolitan District. The occurrence of significant U excesses is a feature of arc magmas, but is typically seen in depleted lavas rather than in highly enriched rocks such as these (~20 ppm Th). This signature requires a recent addition of a U-rich component to the already strongly enriched mantle wedge beneath this region of Italy. We suggest that a supercritical liquid, from deeply subducted carbonate-rich sediments of the still-active Ionian slab, is responsible for generating a high-U, low-Th component, which produces the observed disequilibria. A 30% $^{230}Th$ excess measured in a single unaltered sample from the Lucanian Magmatic Province, along with a less marked negative HFSE anomaly, suggests the contribution of a deeper, garnet-bearing component in the genesis of these magmas, plausibly related to the upwelling of asthenospheric mantle around the corner of the Ionian slab.*

KEY WORDS: *U/Th disequilibria; potassic and ultrapotassic rocks; subduction: metasomatism; mantle melting; Central and Southern Italy*

## INTRODUCTION

Neogene potassic (shoshonitic) and ultrapotassic volcanic rocks are found along the Tyrrhenian Sea margin of the Italian peninsula (Fig. 1). They range from strongly silica-undersaturated to slightly silica-saturated types and are spatially associated with coeval high-K calc-alkalic and calc-alkalic volcanic rocks (Fig. 2). This type of magmatism, which is a common feature of volcanic areas in the Western Mediterranean, is typically associated with destructive plate margins, such as those found in SE Spain (e.g. Venturelli *et al.*, 1984*a*; Duggen *et al.*, 2004), Corsica (Wagner & Velde, 1986), the Western Alps (Venturelli *et al.*, 1984*b*) and the Balkan peninsula (Altherr *et al.*, 2004; Prelević *et al.*, 2004). The parental magmas of the Italian potassic and ultrapotassic volcanic rocks are thought to be generated by partial melting of variably melt-depleted mantle, subsequently modified by metasomatism in either subduction-related (Peccerillo, 1985;

*Corresponding author. Present address: Bristol Isotope Group, Department of Earth Sciences, University of Bristol, Wills Memorial Building, Queen's Road, Bristol BS8 1RJ, UK. Telephone: +44 0117 9545247. Fax: +44 0117 9253385. E-mail: r.avanzinelli@bristol.ac.uk

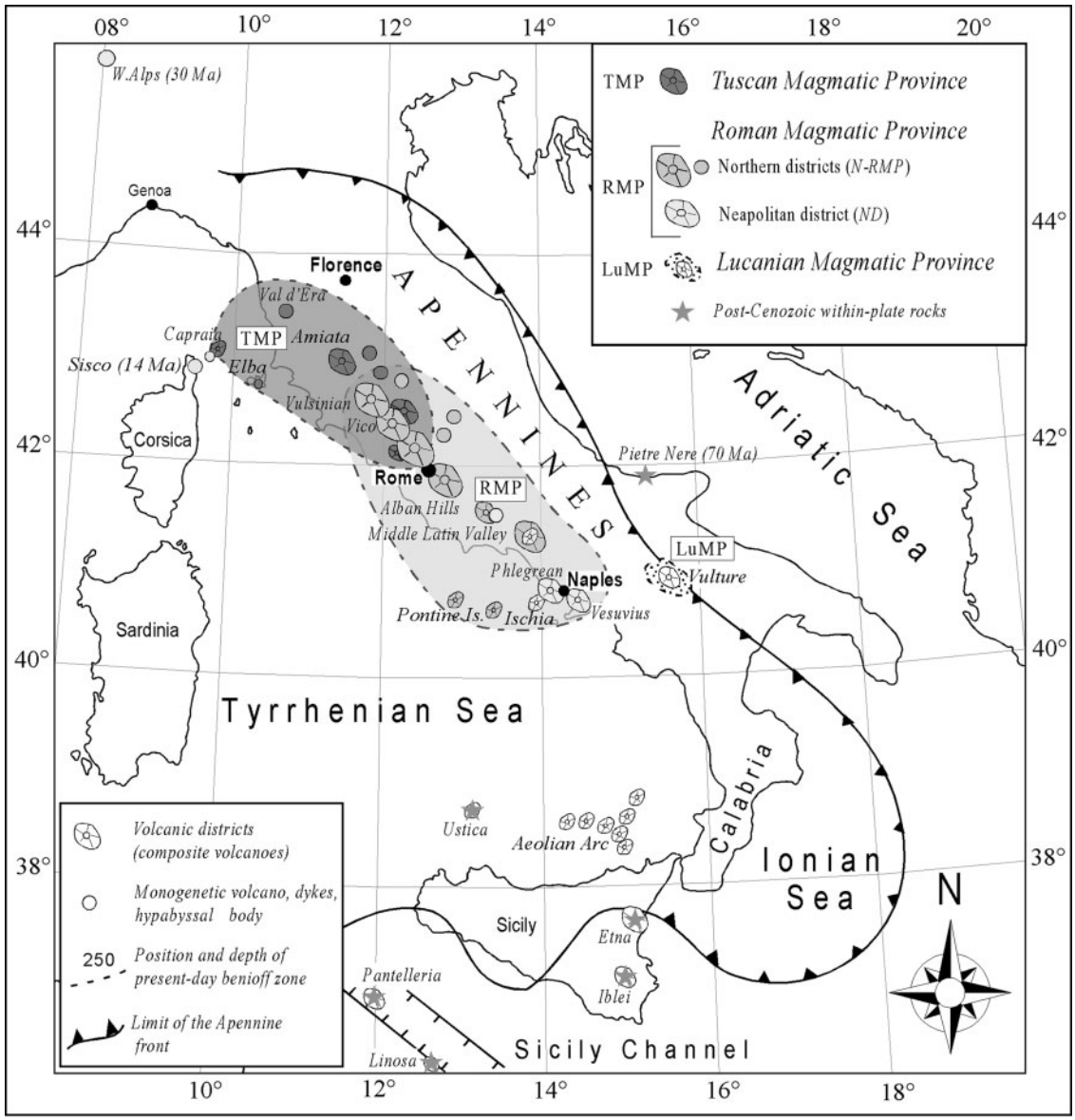


**Fig. 1.** Distribution of the volcanism in Italy. The three encircled areas correspond to: TMP, Tuscan Magmatic Province (dark grey); RMP, Roman Magmatic Province (grey), Neapolitan volcanoes (i.e. ND) are shown with slightly different colour (light grey); LuMP, Lucanian Magmatic Province (dotted). Aeolian Arc calc-alkaline volcanoes are also shown in the Southern Tyrrhenian Sea; grey stars indicate within-plate volcanoes, dykes, and monogenetic volcanoes external to the Apennine front and in the Sicily Channel. In some areas products belonging to different provinces overlap; younger rocks with N-RMP and ND affinity overlap, and postdate rocks with TMP and N-RMP affinity, respectively. Redrawn after Conticelli *et al.* (2007).

Conticelli & Peccerillo, 1992) or within-plate (Gasperini *et al.*, 2002; Bell *et al.*, 2004) geodynamic settings.

A threefold division of Italian potassic and ultrapotassic magmatic rocks (i.e. Tuscan Magmatic Province, Roman Magmatic Province, Lucanian Magmatic Province) based on petrological and geochronological characteristics has been long established (e.g. Washington, 1906; Conticelli *et al.*, 2004). Despite this threefold petrographic division, incompatible trace element data show common features in their relative abundances, notably low concentrations of Nb, Ta and Ti compared with elements of similar incompatibility during normal mantle melting (Fig. 3), henceforth termed 'negative Nb (Ta or Ti) anomalies'. Such distinctive trace element patterns have been widely inferred to be characteristic of a subduction-related signature (e.g. Peccerillo, 1985; Rogers *et al.*, 1985; Conticelli & Peccerillo, 1992; Conticelli *et al.*, 2002, 2007). Additionally, there is a clear geochemical and isotopic gradient from the northernmost region to the southeasternmost region (e.g. Vollmer, 1976; Hawkesworth & Vollmer, 1979;

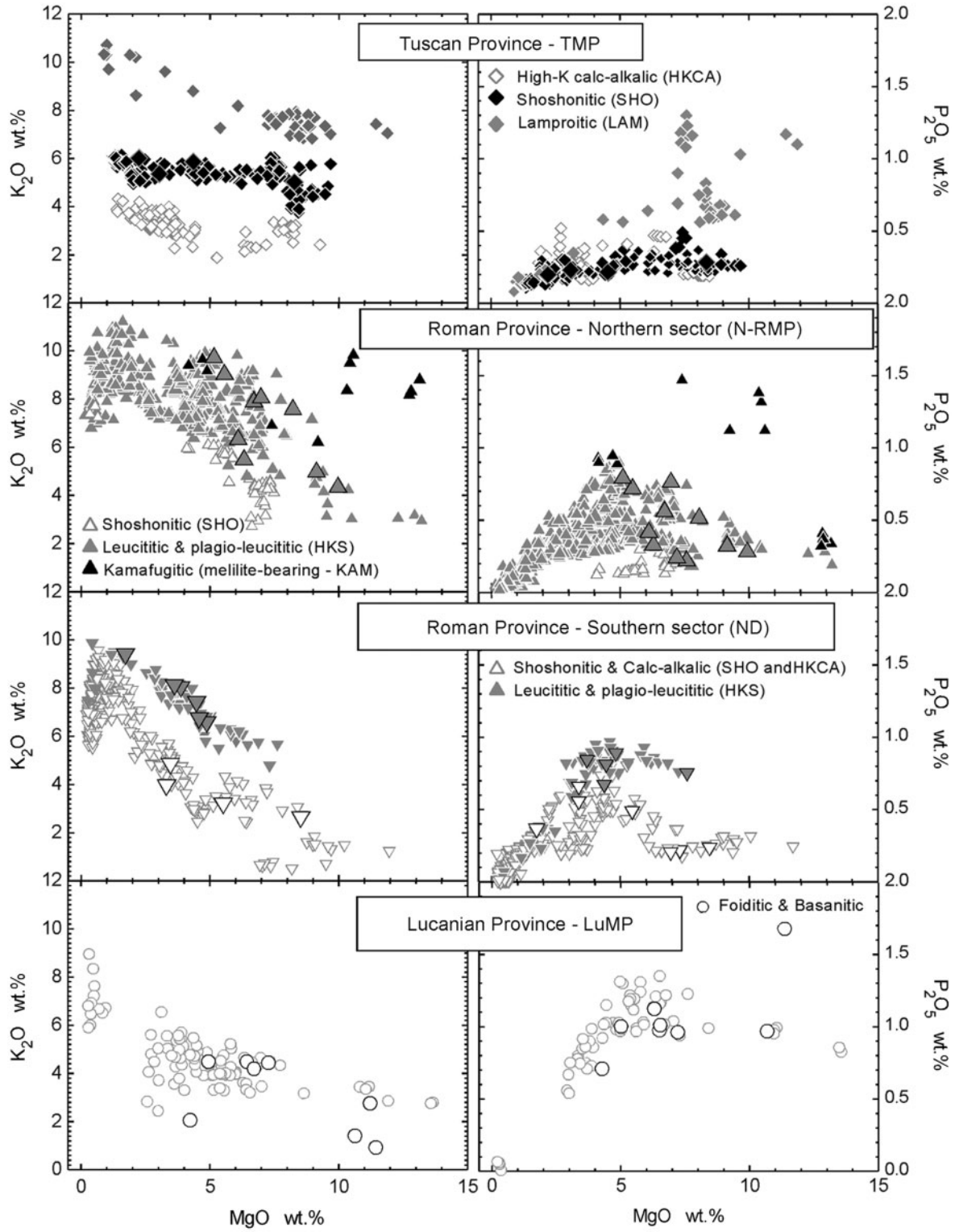


**Fig. 2.** $K_2O$ wt % and $P_2O_5$ wt % vs MgO wt % diagrams showing the evolution pathways for each group of rocks from the different sectors of the Italian peninsula. It should be noted that the upper and lower diagrams are for the northernmost and southernmost sectors of the Italian peninsula, respectively. Data are from Conticelli *et al.* (1991, 1992, 1997, 2002, 2004, 2007), Conticelli (1998), Bindi *et al.* (1999), Perini *et al.* (2003, 2004), Chelazzi *et al.* (2006) and authors' unpublished data. In most of the rocks of the Tuscan, Roman and Lucanian provinces, apatite starts to crystallize and separate at MgO <5 wt %. Samples used in this study are shown as larger symbols.

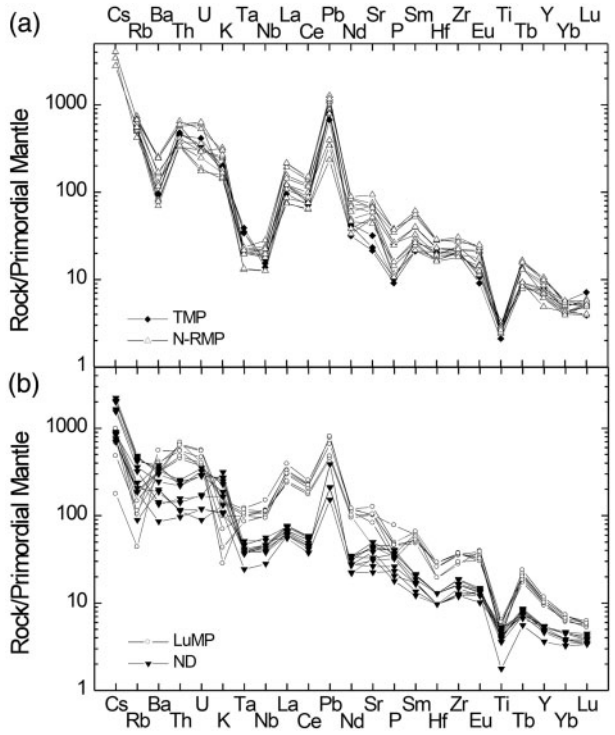


**Fig. 3.** Incompatible trace element patterns normalized to primordial mantle values (Sun & McDonough, 1989).

Vollmer & Hawkesworth, 1980; Gasperini *et al.*, 2002). Hawkesworth & Vollmer (1979) first pointed out this gradient and interpreted the geographical variations as the result of the movement of the Italian plate over a small mantle plume. Recently, others have highlighted the increasing ocean island basalt (OIB)-like character moving southward. This has been interpreted as the response to: (1) a plate window beneath the Southern Tyrrhenian Sea (Gasperini *et al.*, 2002); (2) partial melting of different portions of a mega-plume head based beneath the Tyrrhenian Sea (Bell *et al.*, 2004); (3) the overprinting of a recent subduction-related signature on ancient OIB-source mantle beneath the Neapolitan area (Beccaluva *et al.*, 1991).

Because the processes responsible for the striking chemical compositions of the Tyrrhenian margin volcanic rocks remain hotly debated (e.g. Peccerillo, 1985; Gasperini *et al.*, 2002; Schiano *et al.*, 2004), we have used U–Th disequilibrium measurements to shed new light on their genesis. U and Th are differently fractionated in processes responsible for magma genesis in within-plate and subduction-related environments [see Bourdon & Sims (2003) and Turner *et al.* (2003) for recent reviews on U–Th disequilibria]. Magmas from oceanic and continental within-plate settings are usually characterized by significant $^{230}$Th excesses, as a result of a greater incompatibility of Th during melting (e.g. Gill & Condomines, 1992; Bourdon & Sims, 2003). Subduction-related magmas have rather different U–Th systematics (e.g. Newman *et al.*, 1984; Gill & Williams, 1990) resulting from the combination of processes of mantle melting and addition of fluid or melt from the subducting slab [see recent summary by Turner *et al.* (2003)]. General studies on subduction-related associations (e.g. Condomines *et al.*, 1988; McDermott & Hawkesworth, 1991; Condomines & Sigmarsson, 1993; Hawkesworth *et al.*, 1997) have shown distinctive $^{238}$U excesses in the most fluid-dominated 'depleted' arcs (e.g. Tonga–Kermadec, Marianas), whereas sediment-dominated 'enriched' arcs (e.g. Sunda, Philippines) display values close to radioactive equilibrium. These observations have been argued to reflect preferential addition of U to the arc lava source via slab-derived fluids, which is masked in cases where a significant sedimentary component is also present. However, at high pressures the distinction between slab-derived fluids and melts becomes ambiguous, and they converge to a supercritical liquid [see Hermann *et al.* (2006) for a review]. Using U–Th isotope measurements to investigate Italian magmatism can thus potentially help to elucidate the relationship between subduction and magma genesis in the area.

## GEODYNAMIC SETTING

The geodynamic setting of the Italian region is the result of Africa–Eurasia convergence (Dewey *et al.*, 1989). The Adriatic–Ionian oceanic plate, representing a remnant of the Tethyan domain, has been subducted beneath the Italian peninsula (Faccenna *et al.*, 2001, and references therein). The anti-clockwise rotation of the Corsica–Sardinia block and Italian peninsula, and the formation of back-arc extensional basins (i.e. Liguro-Proveñal and Tyrrhenian basins) have been driven by the roll-back of this NW- to west-dipping subduction zone, which at present is active only beneath Calabria (Fig. 1; Wortel & Spakman, 2000). Alternatively, a slightly more complex model has been suggested, arguing that the present-day position of the Calabrian subduction zone is the result of non-continuous roll-back through repeated events of slab detachment (Carminati *et al.*, 1998; Wortel & Spakman, 2000). This mechanism might also favour inflow of asthenospheric mantle material around the edges of the subducted slab (Wortel & Spakman, 2000). Seismic studies indicate that the Adriatic margin of the Italian peninsula is at present the site of continental collision between the Italian peninsula and the Adriatic microplate (e.g. Anderson & Jackson, 1987*a*; Selvaggi & Chiarabba, 1995). The presence of an active Benioff Zone has been recognized only under the southernmost sector (i.e. Calabria), but some very deep earthquakes are also located beneath the Apennines, suggesting that subduction may be still active beneath the Northern Apennines (Selvaggi &

Amato, 1992). Continuing subduction is characterized by a seismically active, narrow, high-velocity tongue dipping to the NW at a steep angle (Anderson & Jackson, 1987*b*; Wortel & Spakman, 2000; Piromallo & Morelli, 2003).

## OVERVIEW OF THE ITALIAN POTASSIC AND ULTRAPOTASSIC MAGMATISM

K-rich to calc-alkalic magmatism developed diachronously along the Tyrrhenian margin of the Italian peninsula, from southern Tuscany (Plio-Pleistocene), through the Roman and Lucanian provinces (Pleistocene) to the southermost portion of the Roman Province (i.e. Neapolitan District) (Fig. 1).

In the northernmost region of the Italian peninsula (Tuscan Magmatic Province) the volcanic rocks are exclusively leucite-free. They are characterized by high-potassium calc-alkalic (HKCA), shoshonitic (SHO), and silica-rich ultrapotassic lamproitic (LAM) rocks. Beside mantle-derived magmas, orogenic crustally derived granitic magmas are also present (see Savelli, 2000, for a review). The Tuscan lamproites are strongly enriched in $K_2O$ (Fig. 2) and incompatible trace elements and have, along with associated shoshonites, the highest $^{87}Sr/^{86}Sr$ and lowest $^{143}Nd/^{144}Nd$ of the entire Italian region (e.g. Conticelli *et al.*, 2002; Figs 3 and 4). Their isotopic compositions overlap those of upper crustal rocks, but are well within the field of other Mediterranean lamproites related to orogenic-tectonic settings.

The central and southern regions of the Tyrrhenian margin of the Italian peninsula (Roman Magmatic Province, Fig. 1) are characterized by mildly to strongly silica-undersaturated ultrapotassic leucite- (plagio-leucitites and leucitites, HKS) to melilite-bearing rocks (kamafugites, KAM). Minor leucite-free products are erupted both in the early (HKCA) and in the last (SHO) phases of volcanism (e.g. Conticelli *et al.*, 1991, 1997; Perini *et al.*, 2004; Boari & Conticelli, 2008). Roman Province rocks are also strongly enriched in incompatible trace elements, but display less radiogenic Sr isotope compositions than those reported for the Tuscan rocks. Within the Roman Province group, the leucite-bearing rocks (HKS and KAM) have higher $^{87}Sr/^{86}Sr$ than the leucite-free rocks (SHO) (e.g. Conticelli *et al.*, 2002, 2007). Conticelli & Peccerillo (1992) suggested two distinct mantle sources for these magmas.

(1) Tuscan and Roman Province leucite-free magmas have geochemical characteristics that imply derivation from a lithospheric mantle source refertilized by metasomatic fluids derived from recycled crustal material, producing a phlogopite-bearing residual peridotite (Foley, 1992). Melting of this peridotite at low $X_{CO_2}$, with different proportions of vein and ambient mantle, could produce the observed spectrum of leucite-free magmas in the Tuscan region from lamproite to shoshonite and HKCA (Conticelli *et al.*, 2007).

(2) Leucite-bearing Roman Province magmas have also been interpreted as the products of partial melting of lithospheric upper mantle, but with a higher amount of clinopyroxene (Wendlandt & Eggler, 1980*a*, 1980*b*) compared with the Tuscan mantle source. In addition, Conticelli *et al.* (2002) argued that a sedimentary, carbonate-rich component was introduced into their mantle source through subduction. This was required to buffer Sr isotope compositions at ~0·710, raise $X_{CO_2}$, and thus increase the degree of silica undersaturation in the primary melts (Wendlandt & Eggler, 1980*a*).

The southeasternmost volcanic region (Lucanian Magmatic Province) of the Italian peninsula is far from the Tyrrhenian margin, close to the front of the Apennine chain (Fig. 1). This province is characterized by strongly silica-undersaturated volcanic rocks ranging from foiditic melilitites (kamafugites) to basanites. Recently, an inferred subduction-related carbonatitic lava flow has been found at Monte Vulture volcano (D'Orazio *et al.*, 2007).

## SAMPLE SELECTION

Thirty-five samples were selected for isotopic analysis (Table 1), including the most primitive of the recent rocks (<300 ka) from each area: four samples from the leucite-free Tuscan Magmatic Province (Monte Amiata volcano); 13 samples from the youngest volcanic activity of the northernmost districts of the Roman Magmatic Province (Latium area); 10 from the southernmost sector of the Roman Magmatic Province (Neapolitan District); eight from the Lucanian Magmatic Province (Monte Vulture volcano, Monticchio maars). The Monte Amiata volcanic rocks are the only samples from the Tuscan Magmatic Province that are possibly young enough for U–Th analyses. However, it has to be noted that the Monte Amiata rocks do not reflect typical Tuscan magmatic activity, but represent a transitional composition between the Tuscan magmas and the products of the Roman Magmatic Province, in terms of both age and geochemical and isotopic characteristics (Ferrari *et al.*, 1996). The samples of the Roman Magmatic Province belong mostly to the HKS series. Only a few samples from the northernmost districts and some from the Neapolitan District belong to the SHO (leucite-free) series (Table 1). The samples from the Monticchio maars activity are accretionary lapilli that have been individually treated, both mechanically and with an ultrasonic bath, to remove secondary alteration films occurring on the external surfaces.

The nomenclature of the Italian potassic and ultrapotassic rocks is complex and varies both within and between magmatic provinces. For the sake of clarity, we have decided to discriminate between our samples on a simple

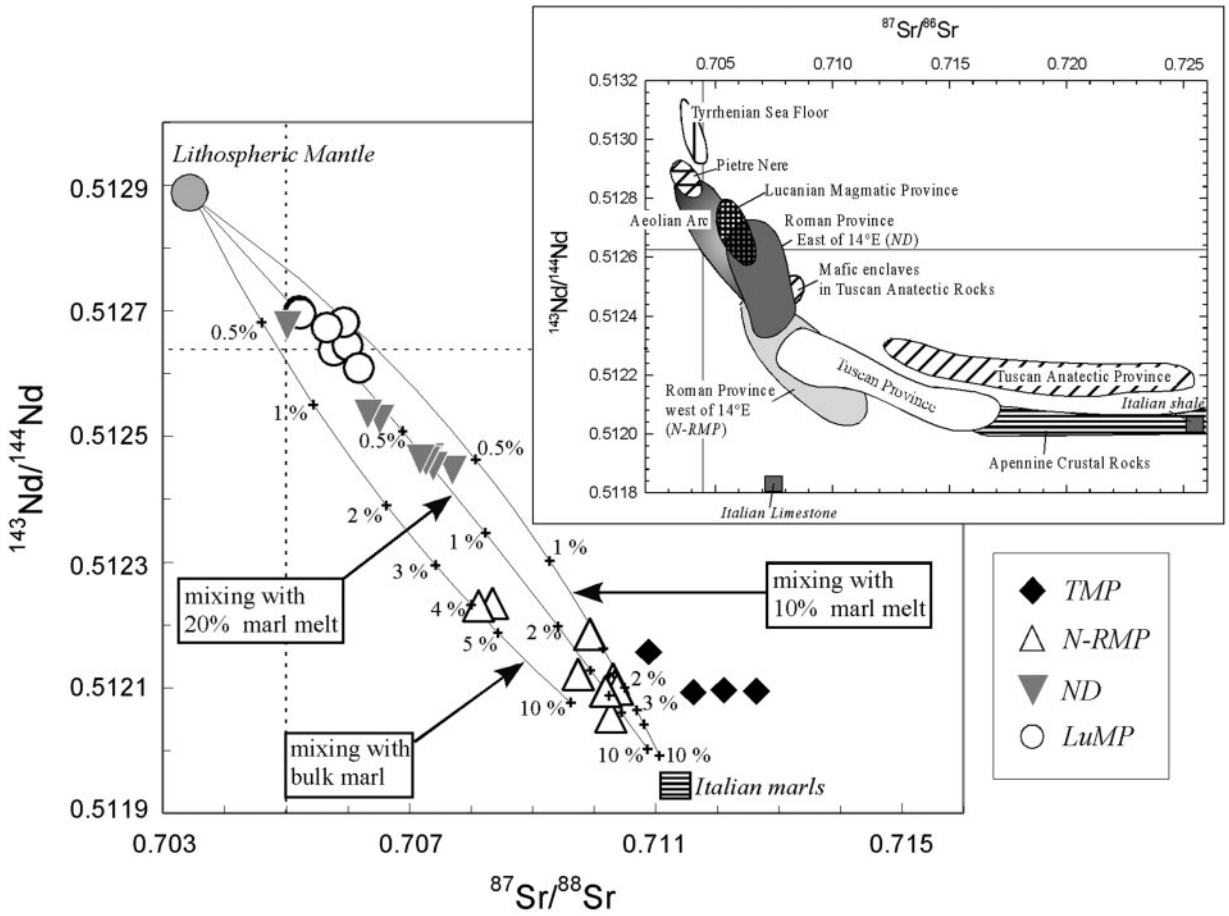


**Fig. 4.** Variation of $^{143}Nd/^{144}Nd$ vs $^{87}Sr/^{86}Sr$ for the Italian potassic and ultrapotassic rocks. Also shown are mixing lines between the pre-enrichment lithospheric mantle and three potential enriching agents represented by bulk sediments and sediment-derived melts corresponding to 10% and 20% of batch melting. The values adopted in the calculation are as follows: mantle end-member: Sr 10 ppm, Nd 0·4 ppm; bulk sediment end-member: Sr 327 ppm, Nd 21·4 ppm. Sediment melts are calculated by batch melting, with $f = 10\%$ and 20%, respectively, the sediment/liquid partition coefficients used in the calculation are $D_{Sr} = 0{\cdot}02$ and $D_{Nd} = 0{\cdot}26$ (see text for further explanation). Mixing lines are drawn only between zero and 10% sediment (or sediment melt) addition, with tick marks at 0·5%, 1%, 2%, 3%, 4%, 5% and 10%. Above 10% the composition of the metasomatized mantle is strongly controlled by that of the sediment component, because of its high Sr and Nd content, and the resulting mixing value would be clustered close to the marl composition (also shown in the diagram) Inset shows other Italian potassic rocks along with Aeolian Arc magmas, Cretaceous within-plate Na-alkali basalts of Punta le Pietre Nere, Tyrrhenian sea-floor basalts, and crustal-derived rhyolites and granitoids from the Tuscan Anatectic Province. Italian limestone and silicic–clastic sediments (Apennine Crustal Rocks) are also shown. Sources of data for these fields have been given by Conticelli *et al.* (2004).

geographical basis. Along with distinctions between the Tuscan Magmatic Province (hereafter TMP), Roman Magmatic Province and Lucanian Magmatic Province (hereafter LuMP), we will subsequently deal separately with samples from the central and northern sectors of the Roman Magmatic Province (i.e. Vulsinian District, Vico District, Colli Albani District, Media Valle Latina District, hereafter N-RMP) from those of the Neapolitan District (e.g. Procida, Somma–Vesuvius and Ischia volcanoes: hereafter ND) because of marked age and trace element differences (e.g. Beccaluva *et al.*, 1991). A list of samples with their location and associated magmatic province is given in Table 1. Major and trace element data are reported in Table 2. Sr–Nd and U–Th isotope data are reported in Table 3. A detailed description of analytical techniques used is given in the Appendix.

## RESULTS

The samples from TMP are silica-saturated to oversaturated shoshonites, with intermediate to high silica ($SiO_2$ 51·5–65·1 wt %) and variable MgO contents (2·2–8·5 wt %). Samples from the N-RMP have generally higher magnesium, lower silica and higher potassium contents than TMP samples, ranging from silica-saturated to strongly silica-undersaturated. Ultrapotassic

*Table 1: Petrography, provenance, and age of selected mafic samples from the Italian volcanic regions*

| Province, volcano | Locality | Sample | Series | Age (ka) | Method | Ref. | Rock type | Petrography |
|---|---|---|---|---|---|---|---|---|
| *LuMP* | | | | | | | | |
| Monticchio maars | Monticchio lakes | VLT 99 | HKS | 132 ± 12 | $^{40}Ar/^{39}Ar$ | 1 | accretionary lapilli | Cpx + Ol(Chr) + Mel + Glass |
| Monticchio maars | Monticchio lakes | VLT 92 | HKS | 132 ± 12 | $^{40}Ar/^{39}Ar$ | 1 | accretionary lapilli | Cpx + Ol(Chr) + Mel + Glass |
| Monticchio maars | Ripacandida | VLT 36 | HKS | 132 ± 12 | $^{40}Ar/^{39}Ar$ | 1 | lapilli fall | Cpx + Lct + Glass |
| Monticchio maars | Ripacandida | VLT 37 | HKS | 132 ± 12 | $^{40}Ar/^{39}Ar$ | 1 | lapilli fall | Cpx + Lct + Glass |
| Monte Vulture | Imbandita | VLT 49 | HKS | 601 ± 7 | $^{40}Ar/^{39}Ar$ | 1 | lava flow | Cpx + Ol + Mag + Lct + Ne + Haü + Glass |
| Monte Vulture | Pedra della Scimmia | VLT 15 | KAM | 601 ± 7 | $^{40}Ar/^{39}Ar$ | 1 | dyke | Ak + Cpx + Mag + Lct + Ne + Ap + Glass |
| Monte Vulture | Foggiano | VLT 19 | HKS | 601 ± 7 | $^{40}Ar/^{39}Ar$ | 1 | lava flow | Ol(Chr) + Cpx + Lct + Ne + Mag + Glass |
| Monte Vulture | Foggiano | VLT 50 | HKS | 601 ± 7 | $^{40}Ar/^{39}Ar$ | 1 | lava flow | Ol(Chr) + Cpx + Lct + Ne + Mag + Glass |
| *RMP—Neapolitan District* | | | | | | | | |
| Vesuvius | AD 1944 eruption | VES 17 | HKS | 0·06 | historical record | — | lava flow | Lct + Cpx + Pl + Ol + Mag + Glass |
| Vesuvius | AD 1858 eruption | VES 18 | HKS | 0·15 | historical record | — | lava flow | Lct + Cpx + Pl + Mag + Glass |
| Vesuvius | Bocca al Viulo | 97VS718*b* | HKS | 1·00 ± 0·04 | archaeomagnetic | 2 | lapilli fall | Cpx + Lct + Ol + Bt + Pl + Glass |
| Vesuvius | Terzigno | 95VS135 | HKS | 1·26 ± 0·03 | $^{14}C$ | 3 | lapilli fall | Cpx + Lct + Pl + Glass |
| Vesuvius | Terzigno | 95VS131 | HKS | 1·26 ± 0·03 | $^{14}C$ | 3 | lapilli fall | Cpx + Lct + Pl + Glass |
| Ischia | Vateliero | I 104 | SHO | 1·6 ± 0·7 | K/Ar | 4 | lava flow | — |
| Ischia | Zaro | I 2SF | SHO | 5·7 ± 1·8 | K/Ar | 4 | lava flow | — |
| Ischia | Grotta di Terra | I 109 | SHO | 22·8 ± 5·2 | K/Ar | 4 | lava flow | — |
| Procida | Acquamorta | FAM | SHO | 55 ± 5 | K/Ar | 5 | scoria fall | Cpx + Ol + Pl + Glass |
| Procida | Procida village | UPFUC | SHO | 21·30 ± 0·17 | Ar–Ar | 6 | pumice | — |
| *RMP—northern districts* | | | | | | | | |
| Vulsini volcanoes | Selva del Lamone | Bols 301 | SHO | 158 ± 5 | K–Ar | 7 | lava flow | Pl + Ol + Cpx + Mag + Glass |
| Vulsini volcanoes | Latera | Bols 282 | HKS | 180 ± 7 | $^{40}Ar/^{39}Ar$ | 7 | lapilli fall | Cpx + Lct + Glass |
| Vulsini volcanoes | Fiordini | VS 189 | HKS | 245·3 ± 4·7 | $^{40}Ar/^{39}Ar$ | 7 | lava flow | Cpx + Ol(Chr) + Lct + Pl + Mag + Glass |
| Vulsini volcanoes | Commenda | VS 67 | HKS | 256 ± 3 | K–Ar | 7 | lava flow | Cpx + Lct + Pl + Mag + Glass |
| Vico volcano | Poggio Varo | VCO 20 | HKS | 120 ± 6 | $^{40}Ar/^{39}Ar$ | 7 | scoria fall | Cpx + Ol + Lct + Pl + Mag + Apa + Glass |
| Vico volcano | Poggio Nibbio | VCO 3 | HKS | 120 ± 6 | $^{40}Ar/^{39}Ar$ | 7 | scoria fall | Cpx + Ol + Lct + Pl + Mag + Apa + Glass |
| Alban Hills volcano | Capo di Bove | VLS 02 | HKS | 277 ± 2 | $^{40}Ar/^{39}Ar$ | 7 | lava flow | Lct + Cpx + Mel + Ne + Mag |
| Alban Hills volcano | Divino Amore | VLS 12 | HKS | 277 ± 2 | $^{40}Ar/^{39}Ar$ | 7 | lava flow | Lct + Cpx + Ne + Apa + Mag + Bt + *Cal* |
| Alban Hills volcano | Colonna | VLS 35 | HKS | 280 ± 5 | $^{40}Ar/^{39}Ar$ | 7 | lava flow | Cpx + Ol + Lct + Mag + Apa |
| Alban Hills volcano | Monte Compatri | VLS 43 | HKS | 280 ± 5 | $^{40}Ar/^{39}Ar$ | 7 | lava flow | Ol(Chr) + Cpx + Lct + Ne + Mag |
| Alban Hills volcano | Osa Pofi–Pozzo | VLS 25 | HKS | 287 ± 6 | $^{40}Ar/^{39}Ar$ | 7 | lava flow | Cpx + Ol(Chr) + Mel + Lct + Ne + Mag |
| Middle Latin Valley | Colonnello | S 18 | HKS | 80 ± 40 | K–Ar | 8 | lava flow | Lct + Cpx + Ol + Pl + Mag + Glass |

(continued)

*Table 1: Continued*

| Province, volcano | Locality | Sample | Series | Age (ka) | Method | Ref. | Rock type | Petrography |
|---|---|---|---|---|---|---|---|---|
| Middle Latin Valley | Colle Spinazzeta | S 9 | SHO | 180 ± 90 | K–Ar | 8 | lava flow | Cpx + Ol(Chr) + Pl + Mag + Lct + Glass |
| *TMP* | | | | | | | | |
| Monte Amiata | Ermeta | AMT 20 | SHO | 209 ± 29 | Fission track | 9 | enclave | Cpx + Ol + Phl + Pl + Sd + Mag + Glass |
| Monte Amiata | Rifugio Macinaie | AMT 82 | SHO | 209 ± 29 | Fission track | 9 | lava flow | Pl + Sd + Cpx + Ol(Chr) + Bt + Opx + Glass |
| Monte Amiata | Rifugio Cantore | AMT 44 | SHO | 203 ± 12 | Fission track | 9 | massive lava flow | Ol(Chr) + Sd + Cpx + Pl + Bt + Glass |
| Monte Amiata | Vetta Amiata | AMT 38 | SHO | 203 ± 12 | Fission track | 9 | dome | Sd + Cpx + Pl + Bt + Ol + Mag + Glass |

LuMP, Lucanian Magmatic Province; RMP, Roman Magmatic Province; TMP, Tuscan Magmatic Province. Magmatic provinces are defined on the basis of the work of Washington (1906) reconsidered by Conticelli *et al*. (2004) following petrological and age criteria. HKS, plagio-leucititic and leucititic Roman-type rocks; KAM, melilite-bearing mafic foidites with kamafugitic affinity; SHO, shoshonitic trachybasalts, shoshonites and olivine latites. Cpx, clinopyroxene; Ol, olivine; Chr, chromite; Mel, melilite; Mag, magnetite; Lct, leucite; Ne, nepheline; Ap, apatite; Pl, plagioclase; Bt, biotite; Cal, calcite; Haü, haüyne. When a mineral abbreviation is given in parentheses, this means that it is enclosed within the previous mineral; when italicized, it is a secondary phase. 'Ref.' column reports age data sources as follows: 1, Brocchini *et al*. (1994); 2, Principe *et al*. (2004); 3, R. Cioni (personal communication); 4, Poli *et al*. (1987); 5, V. Morra (personal communication); 6, Melluso *et al*. (1995); 7, Marra *et al*. (2004); 8, Fornaseri (1986); 9, Bigazzi *et al*. (1981).

plagio-leucitites and leucitites (HKS) are dominant in the N-RMP, although shoshonites are also present (i.e. Vulsini, Middle Latin Valley). Among the ND rocks, only those from Vesuvius are ultrapotassic, whereas the shoshonites from the other volcanoes (i.e. Ischia and Procida) have higher silica and lower potassium contents. Two groups are recognizable among the rocks of the Lucanian Magmatic Province. The older group of >500 ka Monte Vulture lavas are strongly silica-undersaturated basanites with higher $Na_2O$, $TiO_2$ and $P_2O_5$ contents compared with the N-RMP products. The second group, comprising the younger (132 ka) Monte Vulture lavas (Monticchio Lakes samples), are accretionary lapilli produced by phreato-magmatic activity. These lapilli have alkali basaltic compositions with silica contents between 42·7 and 51·5 wt %.

Considered as a whole, the samples analysed in this study have a wide range of major element compositions. $K_2O$, in particular, varies from <1 wt %, in one sample from the Monticchio Lakes (i.e. LuMP), to >9 wt % in samples from the Alban Hills (i.e. N-RMP) (Fig. 2 and Table 2).

Incompatible trace elements are strongly enriched in all of the analysed rocks; primordial mantle normalized trace element patterns are reported in Fig. 3. Strong Nb, Ta, and Ti depletions with respect to other incompatible trace elements are the most striking features of the trace element patterns of the studied samples. Leucite-free and leucite-bearing rocks from the TMP and N-RMP are the most highly enriched in the heavy alkalis (members of the loose geochemical grouping of large ion lithophile elements, LILE), Th and rare earth elements (REE), with deep troughs at Ta, Nb and Ti, the so-called high field strength elements (HFSE). There are also notable troughs at Ba and P. Lower LILE, Th and REE abundances are evident in the ND samples, resulting in smaller LILE/HFSE anomalies. In these samples, the Ba and P troughs are also no longer apparent (Fig. 3). The smallest negative anomalies in Ta and Nb have been measured in the samples from the LuMP, which in contrast show the strongest enrichment in light rare earth elements (LREE) along with the highest LREE/HREE (heavy REE) fractionation. Ba and P troughs are present in the LuMP samples, although they are smaller than in the TMP and N-RMP samples, along with negative anomalies in Rb and K.

Sr and Nd isotope ratios show strong regional variations (Fig. 4). A general northward increase in $^{87}Sr/^{86}Sr$, accompanied by decreasing $^{143}Nd/^{144}Nd$, is observed ranging from 0·7052–0·7062 (LuMP), through 0·7050–0·7077 (ND), to 0·7104 (N-RMP) (Fig. 4). The highest $^{87}Sr/^{86}Sr$ values in our study are found in the Monte Amiata (TMP) rocks (e.g. 0·7116–0·7126), which are, nevertheless, among the lowest values observed in the shoshonitic and lamproitic rocks of the TMP (which have values up to 0·7167, Conticelli *et al*. 1992, 2002).

*Table 2: Major (wt %) and trace (ppm) element concentrations for selected samples from the Italian volcanic regions*

| Province: | Lucanian Magmatic Province (LuMP) | | | | | | | | Roman Magmatic province (RMP)—Neapolitan District | | | | | | | | | |
|---|---|---|---|---|---|---|---|---|---|---|---|---|---|---|---|---|---|---|
| Sample: | VLT 99 | VLT 92 | VLT 36 | VLT 37 | VLT49 | VLT 15 | VLT 19 | VLT 50 | VES 18 | VES 17 | 95VS135 | 95VS131 | 97VS718*b* | I 104 | I 2SF | I 109 | FAM | UPFUC |
| Series: | HKS | HKS | HKS | HKS | HKS | KAM | HKS | HKS | HKS | HKS | HKS | HKS | HKS | SHO | SHO | SHO | SHO | HKS |
| Ref.: | * | * | * | * | * | 1 | 1 | * | * | * | 2 | 2 | 2 | 3 | 3 | 3 | 4 | 4 |
| $SiO_2$ | 42·7 | 50·3 | 49·6 | 51·5 | 47·1 | 44·7 | 47·1 | 47·4 | 49·7 | 48·9 | 48·9 | 48·3 | 48·9 | 54·0 | 52·1 | 52·1 | 52·1 | 58·9 |
| $TiO_2$ | 1·71 | 1·37 | 1·16 | 1·15 | 1·45 | 1·31 | 1·54 | 1·55 | 0·92 | 1·03 | 1·07 | 1·14 | 1·00 | 1·09 | 1·36 | 1·34 | 1·27 | 0·45 |
| $Al_2O_3$ | 12·3 | 16·9 | 18·8 | 19·1 | 17·2 | 18·5 | 15·7 | 15·9 | 19·5 | 19·3 | 16·4 | 16·4 | 13·8 | 17·9 | 18·1 | 18·2 | 15·8 | 19·0 |
| $Fe_2O_3$ | 11·0 | 9·82 | 9·54 | 9·46 | 5·30 | 5·67 | 4·94 | 3·69 | 2·55 | 1·10 | 9·21 | 9·59 | 7·84 | 6·86 | 7·24 | 7·98 | 10·20 | 4·16 |
| FeO | n.d. | n.d. | n.d. | n.d. | 3·35 | 3·02 | 3·26 | 4·38 | 5·21 | 6·71 | n.d. | n.d. | n.d. | n.d. | n.d. | n.d. | n.d. | n.d. |
| MnO | 0·26 | 0·22 | 0·25 | 0·21 | 0·16 | 0·19 | 0·15 | 0·14 | 0·15 | 0·16 | 0·16 | 0·17 | 0·14 | 0·13 | 0·14 | 0·13 | 0·15 | 0·13 |
| MgO | 11·9 | 11·2 | 5·09 | 4·48 | 6·21 | 5·01 | 6·53 | 6·87 | 3·04 | 3·72 | 4·37 | 4·49 | 7·52 | 3·46 | 5·44 | 3·32 | 4·71 | 1·73 |
| CaO | 15·0 | 7·21 | 10·16 | 9·61 | 12·4 | 12·2 | 11·7 | 11·5 | 8·31 | 8·46 | 8·95 | 9·65 | 12·4 | 7·17 | 8·17 | 7·58 | 9·08 | 3·14 |
| $Na_2O$ | 2·51 | 0·66 | 1·44 | 1·64 | 1·45 | 3·88 | 3·79 | 3·04 | 1·59 | 1·54 | 2·69 | 2·49 | 1·89 | 3·78 | 3·78 | 4·68 | 2·82 | 2·61 |
| $K_2O$ | 0·90 | 1·38 | 3·10 | 2·23 | 4·34 | 4·53 | 4·40 | 4·58 | 8·32 | 8·24 | 7·55 | 6·95 | 5·72 | 5·12 | 3·22 | 4·01 | 3·42 | 9·52 |
| $P_2O_5$ | 1·68 | 0·99 | 0·79 | 0·70 | 1·04 | 1·00 | 0·97 | 0·96 | 0·70 | 0·84 | 0·77 | 0·82 | 0·76 | 0·55 | 0·48 | 0·67 | 0·44 | 0·37 |
| LOI | 4·19 | 5·11 | 3·35 | 5·14 | 1·47 | 1·81 | 0·47 | 0·65 | 0·59 | 0·24 | 0·40 | 0·28 | 0·89 | 0·85 | 0·31 | 0·96 | 3·65 | 1·44 |
| Mg-no. | 71·4 | 72·6 | 55·4 | 52·5 | 61·6 | 56·4 | 64·0 | 65·2 | 45·9 | 50·3 | 52·5 | 52·2 | 69·1 | 54·0 | 63·7 | 49·2 | 51·8 | 49·2 |
| Sc | 32·7 | n.d. | n.d. | 13·7 | 26·1 | 18·8 | 25·3 | 25·9 | n.d. | n.d. | n.d. | n.d. | n.d. | 15·0 | 20·8 | 16·2 | 20·1 | 5·6 |
| V | 218 | 203 | 236 | 200 | 228 | 265 | 207 | 203 | 194 | 230 | 242 | 268 | 228 | 164 | 166 | 229 | 237 | 74 |
| Cr | 309 | n.d. | n.d. | 15 | 42 | 16 | 134 | 84 | n.d. | n.d. | 48 | 30 | 218 | 59 | 145 | 23 | 5 | 4 |
| Co | 38·2 | 45·4 | 24·6 | 21·4 | 26·9 | 23·3 | 26·3 | 26·2 | 21·1 | 22·7 | 24·5 | 26·2 | 25·9 | 15·7 | 20·1 | 17·7 | 27·4 | 5·2 |
| Ni | 182 | 417 | 27 | 18 | 27 | 16 | 35 | 47 | 19 | 26 | 28 | 33 | 66 | 24 | 57 | 16 | 23 | 5 |
| Cu | 47 | 58 | 76 | 85 | 63 | 86 | 60 | 60 | 99 | 101 | 119 | 112 | 68 | 71 | 20 | 61 | 56 | 9 |
| Zn | 89 | n.d. | n.d. | 98 | 88 | 105 | 85 | 83 | n.d. | n.d. | n.d. | n.d. | n.d. | n.d. | n.d. | n.d. | n.d. | 70 |
| Ga | 15 | 16 | 19 | 20 | 19 | 22 | 19 | 19 | 15 | 15 | 15 | 16 | 12 | 14 | 14 | 15 | 15 | 13 |
| Rb | 28 | 66 | 93 | 72 | 142 | 137 | 117 | 124 | 278 | 307 | 266 | 290 | 227 | 151 | 118 | 57 | 131 | 204 |
| Sr | 2130 | 954 | 2170 | 1740 | 2660 | 2810 | 2180 | 2190 | 941 | 885 | 1050 | 933 | 694 | 556 | 475 | 648 | 814 | 694 |
| Y | 48·5 | 42·9 | 49·0 | 46 | 53 | 60 | 46 | 46 | 21 | 23 | 24 | 25 | 22 | 24 | 24 | 24 | 24 | 16 |
| Zr | 312 | 331 | 392 | 411 | 406 | 445 | 418 | 413 | 182 | 206 | 210 | 185 | 180 | 165 | 137 | 143 | 133 | 140 |
| Nb | 107 | 71 | 78 | 82 | 67 | 139 | 81 | 80 | 32 | 40 | 33 | 33 | 32 | 28 | 37 | 30 | 20 | 27 |
| Cs | 1·4 | 7·8 | 5·9 | 3·8 | 6·5 | 6·7 | 5·4 | 5·4 | 15·8 | 17·5 | 13·0 | 16·2 | 12·2 | 7·2 | 6·9 | 6·0 | 5·5 | 6·7 |
| Ba | 2900 | 3890 | 2250 | 2050 | 2740 | 2330 | 2210 | 2270 | 2440 | 2090 | 2630 | 2290 | 1710 | 944 | 600 | 1390 | 1310 | 998 |
| La | 268 | 203 | 228 | 223 | 208 | 190 | 162 | 170 | 50·6 | 51·3 | 52·6 | 46·6 | 46·0 | 44·5 | 37·9 | 42·4 | 40·7 | 41·2 |
| Ce | 449 | 366 | 412 | 400 | 397 | 371 | 311 | 327 | 98·5 | 102 | 104 | 93·3 | 94·0 | 86 | 66·7 | 80·9 | 79·1 | 73·8 |
| Pr | 49·7 | 38·4 | 46·1 | 45·1 | 46·0 | 42·1 | 36·2 | 38·5 | 11·7 | 12·5 | 12·6 | 11·7 | 11·7 | 10·5 | 8·31 | 9·66 | 9·88 | 8·47 |
| Nd | 163 | 132 | 160 | 151 | 163 | 150 | 128 | 136 | 42·2 | 47·1 | 46·6 | 45·0 | 45·3 | 37·5 | 30·3 | 36·8 | 37·6 | 29·7 |
| Sm | 26·9 | 21·4 | 27·3 | 25·30 | 29·1 | 28·0 | 22·6 | 23·5 | 8·3 | 9·4 | 9·3 | 9·1 | 9·5 | 7·4 | 6·0 | 7·3 | 7·6 | 5·4 |
| Eu | 6·62 | 5·19 | 6·02 | 5·57 | 6·52 | 6·36 | 5·06 | 5·39 | 2·20 | 2·37 | 2·49 | 2·39 | 2·27 | 2·03 | 1·70 | 2·25 | 2·29 | 2·03 |
| Gd | 22·0 | 18·1 | 21·5 | 20·2 | 24·3 | 25·1 | 19·2 | 20·0 | 6·98 | 7·76 | 8·16 | 8·24 | 8·20 | 7·02 | 5·77 | 6·81 | 7·09 | 5·03 |
| Tb | 2·25 | 1·87 | 2·34 | 2·15 | 2·56 | 2·68 | 2·00 | 2·16 | 0·78 | 0·85 | 0·90 | 0·93 | 0·92 | 0·80 | 0·72 | 0·81 | 0·86 | 0·60 |
| Dy | 10·2 | 8·49 | 10·5 | 9·52 | 11·6 | 13·1 | 9·14 | 9·99 | 3·99 | 4·25 | 4·50 | 5·00 | 4·23 | 4·50 | 4·25 | 4·40 | 4·54 | 3·21 |

(continued)

*Table 2: Continued*

| Province: | Lucanian Magmatic Province (LuMP) | | | | | | | | Roman Magmatic province (RMP)—Neapolitan District | | | | | | | | | |
|---|---|---|---|---|---|---|---|---|---|---|---|---|---|---|---|---|---|---|
| Sample: | VLT 99 | VLT 92 | VLT 36 | VLT 37 | VLT49 | VLT 15 | VLT 19 | VLT 50 | VES 18 | VES 17 | 95VS135 | 95VS131 | 97VS718*b* | I 104 | I 2SF | I 109 | FAM | UPFUC |
| Series: | HKS | HKS | HKS | HKS | HKS | KAM | HKS | HKS | HKS | HKS | HKS | HKS | HKS | SHO | SHO | SHO | SHO | HKS |
| Ref.: | * | * | * | * | * | 1 | 1 | * | * | * | 2 | 2 | 2 | 3 | 3 | 3 | 4 | 4 |
| Ho | 1·70 | 1·43 | 1·64 | 1·55 | 1·88 | 2·11 | 1·55 | 1·62 | 0·75 | 0·75 | 0·80 | 0·87 | 0·77 | 0·83 | 0·81 | 0·90 | 0·81 | 0·58 |
| Er | 4·57 | 3·78 | 4·26 | 4·06 | 4·87 | 5·36 | 4·03 | 4·36 | 2·06 | 2·13 | 2·29 | 2·44 | 2·20 | 2·47 | 2·41 | 2·56 | 2·31 | 1·68 |
| Tm | 0·51 | 0·49 | 0·48 | 0·45 | 0·56 | 0·61 | 0·49 | 0·50 | 0·27 | 0·26 | 0·29 | 0·33 | 0·25 | 0·31 | 0·33 | 0·31 | 0·28 | 0·23 |
| Yb | 3·5 | 3·2 | 3·5 | 3·0 | 3·6 | 4·0 | 3·1 | 3·3 | 1·8 | 1·9 | 2·2 | 2·2 | 1·9 | 2·3 | 2·2 | 2·3 | 1·9 | 1·6 |
| Lu | 0·43 | 0·39 | 0·46 | 0·42 | 0·43 | 0·50 | 0·41 | 0·43 | 0·25 | 0·25 | 0·28 | 0·28 | 0·26 | 0·29 | 0·31 | 0·33 | 0·28 | 0·25 |
| Hf | 6·0 | 6·0 | 8·0 | 8·0 | 9·0 | 9·0 | 9·0 | 9·0 | 4·0 | 4·0 | 4·0 | 4·0 | 4·0 | 3·0 | 3·0 | 3·0 | 3·0 | 3·0 |
| Ta | 5·0 | 3·5 | 4·1 | 4·1 | 4·1 | 5·7 | 4·4 | 4·8 | 1·5 | 1·9 | 1·6 | 1·7 | 1·6 | 1·6 | 2·1 | 1·6 | 1·0 | 1·6 |
| Pb | 55·1 | n.d. | n.d. | 57·3 | 46·6 | 12·6 | 32·0 | 34·0 | n.d. | n.d. | n.d. | n.d. | n.d. | n.d. | 10·8 | 15·0 | 14·8 | 27·5 |
| Th | 47·0 | 46·4 | 56·5 | 58·4 | 54·5 | 44·9 | 38·2 | 40·7 | 20·7 | 20·4 | 18·7 | 21·8 | 18·7 | 13·3 | 8·2 | 9·6 | 9·9 | 12·0 |
| U | 9·73 | 7·54 | 11·8 | 8·44 | 11·5 | 12·8 | 7·77 | 8·44 | 5·94 | 5·99 | 6·74 | 7·35 | 6·07 | 3·49 | 2·51 | 1·87 | 2·50 | 3·64 |

| Province: | Roman Magmatic Province (RMP)—northern districts | | | | | | | | | | | | | Tuscan Magmatic Province (TMP) | | | |
|---|---|---|---|---|---|---|---|---|---|---|---|---|---|---|---|---|---|
| Sample: | Bols 301 | VCO 20 | VCO 3 | S 18 | Bols 282 | S 9 | VS 189 | VLS 02 | VLS 35 | VLS 43 | VLS 12 | VLS 25 | VS 67 | AMT 20 | AMT 82 | AMT 44 | AMT 38 |
| Series: | SHO | HKS | HKS | HKS | HKS | SHO | HKS | HKS | HKS | HKS | HKS | HKS | HKS | SHO | SHO | SHO | SHO |
| Ref.: | 6 | 7 | 7 | 8 | 9 | 8 | 5 | 10 | 10 | 10 | 10 | 10 | 5 | * | * | * | * |
| $SiO_2$ | 53·7 | 47·5 | 49·5 | 47·7 | 49·1 | 48·8 | 50·3 | 48·1 | 49·3 | 47·6 | 47·2 | 44·8 | 47·7 | 51·5 | 59·2 | 62·7 | 65·1 |
| $TiO_2$ | 0·72 | 0·73 | 0·77 | 0·72 | 0·84 | 0·77 | 0·62 | 0·76 | 0·64 | 0·69 | 0·76 | 0·72 | 0·67 | 0·79 | 0·65 | 0·68 | 0·54 |
| $Al_2O_3$ | 18·0 | 16·0 | 16·1 | 18·0 | 15·2 | 16·5 | 15·5 | 16·1 | 14·5 | 15·2 | 17·2 | 16·0 | 14·3 | 15·8 | 16·6 | 17·0 | 16·7 |
| $Fe_2O_3$ | 1·58 | 7·71 | 4·29 | 1·77 | 5·13 | 2·34 | 1·34 | 2·38 | 2·74 | 2·64 | 3·72 | 3·16 | 2·58 | 4·41 | 1·01 | 1·18 | 0·87 |
| FeO | 3·94 | 0·97 | 3·79 | 4·29 | 2·46 | 4·57 | 4·82 | 5·30 | 4·39 | 4·35 | 3·62 | 5·71 | 4·72 | 2·67 | 4·01 | 3·27 | 2·79 |
| MnO | 0·11 | 0·16 | 0·15 | 0·13 | 0·13 | 0·15 | 0·15 | 0·14 | 0·13 | 0·11 | 0·15 | 0·14 | 0·14 | 0·12 | 0·08 | 0·08 | 0·06 |
| MgO | 7·04 | 7·26 | 7·65 | 6·40 | 6·31 | 9·09 | 10·02 | 5·21 | 6·85 | 8·20 | 5·51 | 7·06 | 9·19 | 8·50 | 4·46 | 3·12 | 2·21 |
| CaO | 7·64 | 13·7 | 11·1 | 10·6 | 13·2 | 12·1 | 10·5 | 9·27 | 11·0 | 11·7 | 10·19 | 11·17 | 13·9 | 9·8 | 5·96 | 4·30 | 3·35 |
| $Na_2O$ | 2·54 | 1·45 | 1·60 | 2·52 | 1·63 | 2·81 | 1·88 | 2·04 | 1·62 | 1·24 | 1·73 | 2·22 | 1·41 | 1·02 | 1·83 | 1·84 | 1·97 |
| $K_2O$ | 4·57 | 4·35 | 4·82 | 7·40 | 5·59 | 2·62 | 4·51 | 9·87 | 8·17 | 7·75 | 9·23 | 8·22 | 5·10 | 5·14 | 5·94 | 5·58 | 6·17 |
| $P_2O_5$ | 0·21 | 0·24 | 0·22 | 0·54 | 0·33 | 0·27 | 0·30 | 0·80 | 0·56 | 0·52 | 0·72 | 0·78 | 0·33 | 0·28 | 0·21 | 0·22 | 0·19 |
| LOI | 0·53 | 0·95 | 0·64 | 0·57 | 0·96 | 0·62 | 0·91 | 1·11 | 2·07 | 1·21 | 0·94 | 1·46 | 0·73 | 2·48 | 0·74 | 1·91 | 1·06 |
| Mg-no. | 73·4 | 65·7 | 67·6 | 69·5 | 65·2 | 74·0 | 77·7 | 59·4 | 67·6 | 71·8 | 62·4 | 63·4 | 73·2 | 72·6 | 65·5 | 60·2 | 56·4 |
| Sc | 23·4 | *25·8* | *36·1* | *27·0* | *24·1* | *36·0* | *26·3* | *17·9* | 27·0 | *39·7* | *17·7* | *20·1* | *38·1* | 37·2 | *18·2* | *14·6* | *13·0* |
| V | 152 | *206* | *255* | *233* | n.d. | *233* | *202* | *306* | 234 | *238* | *288* | *290* | n.d. | 183 | *109* | *91* | *69* |
| Cr | 508 | *244* | *206* | *151* | *234* | *490* | *476* | *18* | 133 | *206* | *23* | *29* | *516* | 873 | *156* | *88* | *49* |
| Co | 30·0 | *35·0* | *32·5* | *32·0* | *28·4* | *40·0* | *37·0* | *33·5* | 34·0 | *37·9* | *33·3* | *37·1* | *42·0* | 31·0 | *18·1* | *14·3* | *8·87* |

(continued)

*Table 2: Continued*

| Province: | Roman Magmatic Province (RMP)—northern districts | | | | | | | | | | | | | Tuscan Magmatic Province (TMP) | | | |
|---|---|---|---|---|---|---|---|---|---|---|---|---|---|---|---|---|---|
| Sample: | Bols 301 | VCO 20 | VCO 3 | S 18 | Bols 282 | S 9 | VS 189 | VLS 02 | VLS 35 | VLS 43 | VLS 12 | VLS 25 | VS 67 | AMT 20 | AMT 82 | AMT 44 | AMT 38 |
| Series: | SHO | HKS | HKS | HKS | HKS | SHO | HKS | HKS | HKS | HKS | HKS | HKS | HKS | SHO | SHO | SHO | SHO |
| Ref.: | 6 | 7 | 7 | 8 | 9 | 8 | 5 | 10 | 10 | 10 | 10 | 10 | 5 | * | * | * | * |
| Ni | 128 | *87* | *79* | *58* | n.d. | *87* | *180* | *46* | 83 | *96* | *44* | *48* | *125* | 99 | *56* | *37* | *25* |
| Cu | 30 | *75* | *65* | n.d. | n.d. | n.d. | *56* | *133* | 63 | *66* | *115* | *133* | n.d. | 43 | *41* | *20* | *14* |
| Zn | 60 | *72* | *67* | n.d. | n.d. | n.d. | *63* | *74* | 76 | *58* | *75* | *74* | n.d. | 67 | *62* | *59* | *52* |
| Ga | 15 | n.d. | n.d. | n.d. | n.d. | n.d. | *11* | n.d. | 13 | n.d. | n.d. | n.d. | n.d. | 21 | n.d. | n.d. | n.d. |
| Rb | 272 | *316* | *348* | *332* | *349* | *112* | *266* | *471* | 440 | *386* | *438* | *425* | *353* | 269 | *320* | *325* | *366* |
| Sr | 444 | *1065* | *1063* | *1492* | *1239* | *848* | *1085* | *1579* | 1462 | *1235* | *1402* | *1973* | *916* | 708 | *671* | *493* | *454* |
| Y | 24 | *35* | *33* | *31* | *28* | *20* | *22* | *47* | 42 | *39* | *48* | *45* | *28* | 73 | *34* | *36* | *30* |
| Zr | 228 | *237* | *221* | *218* | *268* | *86* | *225* | *320* | 245 | *251* | *342* | *302* | *203* | 236 | *242* | *240* | *225* |
| Nb | 14·8 | *13* | *13* | *9* | *16* | *8* | *15* | *17* | 14 | *14* | *20* | *16* | *9* | 12 | *12* | *11* | *10* |
| Cs | 24·2 | n.d. | n.d. | n.d. | n.d. | n.d. | *27·0* | n.d. | 31·9 | n.d. | n.d. | n.d. | *22·0* | 21·0 | n.d. | n.d. | n.d. |
| Ba | 442 | *486* | *576* | *892* | *890* | *848* | *824* | *1709* | 1127 | *1189* | *1787* | *1721* | *550* | 790 | *652* | *678* | *667* |
| La | 70·6 | *52* | *51* | *83* | *74* | *33* | *83* | *133* | 107 | *99* | *147* | *148* | *59* | 138 | *82·2* | *82·7* | *65·6* |
| Ce | 134 | *112* | *115* | *177* | *150* | *68* | *156* | *246* | 216 | *205* | *258* | *267* | *134* | 160 | *136* | *144* | *127* |
| Pr | 13·4 | n.d. | n.d. | n.d. | n.d. | n.d. | n.d. | n.d. | 27·1 | n.d. | n.d. | n.d. | n.d. | 38·3 | n.d. | n.d. | n.d. |
| Nd | 47 | *45* | *45* | *81* | *66* | *30* | *52* | *115* | 98·7 | *93* | *113* | *120* | *63* | 152 | *58·0* | *56·0* | *43·0* |
| Sm | 7·89 | *9·50* | *9·60* | *14·5* | *12·8* | *6·40* | *10·9* | *23·3* | 17·6 | *17·8* | *24·7* | *27·0* | *11·8* | 31·9 | *12·3* | *11·6* | *9·40* |
| Eu | 1·66 | *1·90* | *2·05* | *3·00* | *2·50* | *1·53* | *2·10* | *3·88* | 3·49 | *3·60* | *3·93* | *4·19* | *2·41* | 4·57 | *1·80* | *1·80* | *1·53* |
| Gd | 5·80 | n.d. | n.d. | n.d. | n.d. | n.d. | n.d. | n.d. | 13·7 | n.d. | n.d. | n.d. | n.d. | 24·7 | n.d. | n.d. | n.d. |
| Tb | 0·87 | *0·84* | *0·90* | *1·50* | *1·00* | *0·70* | *1·00* | *1·79* | 1·45 | *1·40* | *1·69* | *1·70* | *1·00* | 3·20 | *1·00* | *1·00* | *0·90* |
| Dy | 4·78 | n.d. | n.d. | n.d. | n.d. | n.d. | n.d. | n.d. | 6·60 | n.d. | n.d. | n.d. | n.d. | 17·5 | n.d. | n.d. | n.d. |
| Ho | 0·89 | n.d. | n.d. | n.d. | n.d. | n.d. | n.d. | n.d. | 1·10 | n.d. | n.d. | n.d. | n.d. | 2·88 | n.d. | n.d. | n.d. |
| Er | 2·58 | n.d. | n.d. | n.d. | n.d. | n.d. | n.d. | n.d. | 2·95 | n.d. | n.d. | n.d. | n.d. | 8·00 | n.d. | n.d. | n.d. |
| Tm | 0·40 | n.d. | n.d. | n.d. | n.d. | n.d. | n.d. | n.d. | 0·35 | n.d. | n.d. | n.d. | n.d. | 1·00 | n.d. | n.d. | n.d. |
| Yb | 2·57 | *2·4* | *2·1* | *2·5* | *2·1* | *1·9* | *2·1* | *2·7* | 2·20 | *2·1* | *2·8* | *2·8* | *1·9* | 6·40 | *2·6* | *2·8* | *2·0* |
| Lu | 0·37 | *0·44* | *0·39* | *0·41* | *0·37* | *0·29* | *0·36* | *0·36* | 0·29 | *0·30* | *0·38* | *0·42* | *0·38* | 0·93 | *0·38* | *0·53* | *0·29* |
| Hf | 6·2 | *5·1* | *5·6* | *6·1* | *5·9* | *2·7* | *5·2* | *8·6* | 7·0 | *7·1* | *8·7* | *8·9* | *5·0* | 5·1 | *6·3* | *7·0* | *6·4* |
| Ta | 1·01 | *0·86* | *0·83* | *0·53* | *0·81* | *0·56* | *0·91* | *0·92* | 0·80 | *0·80* | *0·96* | *0·89* | *0·55* | 0·70 | *1·40* | *1·60* | *1·45* |
| Pb | 41·0 | *17* | *24* | *28* | n.d. | *9·7* | *63* | *78* | 57 | *56* | *90* | *83* | n.d. | 29 | *48* | *58* | *62* |
| Th | 41·2 | *29·3* | *28·3* | *28·0* | *32·0* | *9·7* | *48·4* | *49·5* | 35·0 | *31·9* | *55·5* | *50·5* | *28·9* | 24·0 | *38·0* | *40·8* | *39·5* |
| U | 6·58 | *3·9* | *3·6* | *6·4* | *7·6* | *3·0* | *12·6* | *6·2* | 6·14 | n.d. | *11·1* | *13·2* | *5·2* | 7·8 | *8·7* | *7·1* | *7·3* |

Mg-number $= 100 \times [Mg/(Mg + 0{\cdot}85Fe_{tot})]$. 'Ref.' row refers to data source and samples provider, as follows: 1, major elements from Bindi *et al*. (1999); 2, samples supplied by R. Cioni; 3, samples provided by E. Morra, major element data from Di Girolamo *et al*. (1995); 4, samples provided by L. Melluso, major element data from Melluso *et al*. (1995); 5, major and some trace elements from Conticelli & Peccerillo (1992); 6, major and some trace elements from Conticelli *et al*. (1991); 7, major and some trace elements from Perini *et al*. (2004); 8, major and some trace elements from Conticelli *et al*. (2002, 2007); 9, major and some trace elements from Conticelli & Peccerillo (1992); 10, major and some trace elements from E. Boari (personal communication); *, samples collected by the authors, unpublished data. Major elements are water-free normalized; LOI, loss on ignition, is separately reported. Trace element values in italics have been determined using coupled XRF (V, Cr, Ni, Cu, Zn, Rb, Sr, Y, Zr, Nb, Ba), ICP-MS (U, Th, Pb) and INAA methods (REE, Hf, Ta, Th). n.d., not analysed. Bias between the analytical methods has been checked using international reference samples as unknown, and it has been found to be within analytical error.

*Table 3: Sr, Nd and U–Th isotopic data for the selected samples from the Italian volcanic regions*

| Province, volcano | Sample | Age (ka) | $^{87}Sr/^{86}Sr$ | 2 σm | $^{143}Nd/^{144}Nd$ | 2 σm | U (ppm) | Th (ppm) | $(^{234}U/^{238}U)$ | 2 σm | $(^{238}U/^{232}Th)$ | 2 σm | Measured values | | | | Age-corrected values | | | |
|---|---|---|---|---|---|---|---|---|---|---|---|---|---|---|---|---|---|---|---|---|
| | | | | | | | | | | | | | $(^{230}Th/^{232}Th)_m$ | 2 σm | $(^{230}Th/^{238}U)_m$ | 2 σm | $(^{230}Th/^{232}Th)_i$ | 2 σm | $(^{230}Th/^{238}U)_i$ | 2 σm |
| *LuMP* | | | | | | | | | | | | | | | | | | | | |
| Monticchio | VLT 99 | 132 ± 12 | 0·705786 | ±6 | 0·512636 | ±5 | 10·14 | 44·57 | 0·992 | 0·003 | 0·691 | 0·002 | 0·752 | 0·004 | 1·089 | 0·003 | 0·896 | 0·023 | 1·297 | 0·035 |
| Monticchio | VLT 92 | 132 ± 12 | 0·706008 | ±6 | 0·512644 | ±6 | 8·49 | 47·43 | 0·968 | 0·003 | 0·544 | 0·002 | 0·617 | 0·003 | 1·134 | 0·004 | — | — | altered | — |
| Monticchio | VLT 37 | 132 ± 12 | 0·705949 | ±7 | 0·512681 | ±6 | 8·23 | 50·62 | 0·987 | 0·003 | 0·493 | 0·002 | 0·611 | 0·003 | 1·239 | 0·004 | — | — | altered | — |
| Vulture | VLT 49 | 601 ± 7 | 0·705675 | ±8 | 0·512672 | ±6 | — | — | — | — | — | — | — | — | — | — | — | — | — | — |
| Vulture | VLT 15 | 601 ± 7 | 0·706189 | ±7 | 0·512608 | ±5 | — | — | — | — | — | — | — | — | — | — | — | — | — | — |
| Vulture | VLT 19 | 601 ± 7 | 0·705223 | ±7 | 0·512698 | ±5 | — | — | — | — | — | — | — | — | — | — | — | — | — | — |
| Vulture | VLT 50 | 601 ± 7 | 0·705246 | ±6 | 0·512695 | ±7 | — | — | — | — | — | — | — | — | — | — | — | — | — | — |
| *RMP—Neapolitan District* | | | | | | | | | | | | | | | | | | | | |
| Vesuvius | VES 17 | 0·06 | 0·707228 | ±5 | 0·512474 | ±6 | 6·30 | 19·45 | 1·001 | 0·003 | 0·983 | 0·005 | 0·868 | 0·005 | 0·884 | 0·004 | 0·868 | 0·005 | 0·884 | 0·004 |
| Vesuvius | VES 18 | 0·154 | 0·707437 | ±9 | 0·512462 | ±4 | 6·34 | 20·17 | 1·001 | 0·003 | 0·953 | 0·004 | 0·878 | 0·005 | 0·921 | 0·003 | 0·878 | 0·004 | 0·921 | 0·003 |
| Vesuvius | VS 95 135 | 1·26 ± 0·03 | 0·707325 | ±7 | 0·512477 | ±6 | 6·70 | 16·76 | 0·999 | 0·003 | 1·215 | 0·006 | 0·887 | 0·005 | 0·730 | 0·003 | 0·884 | 0·005 | 0·728 | 0·003 |
| Vesuvius | VS 95 131 | 1·26 ± 0·03 | — | — | — | — | 7·60 | 20·78 | 1·003 | 0·004 | 1·112 | 0·006 | 0·896 | 0·005 | 0·806 | 0·003 | 0·894 | 0·005 | 0·804 | 0·004 |
| Vesuvius | VS 97-718*b* | 1·00 ± 0·04 | 0·707729 | ±9 | 0·512458 | ±5 | 6·23 | 17·49 | 1·002 | 0·004 | 1·083 | 0·005 | 0·882 | 0·006 | 0·815 | 0·003 | 0·880 | 0·005 | 0·813 | 0·004 |
| Ischia | I 104 | 1·6 ± 0·7 | 0·706354 | ±6 | 0·512543 | ±5 | 3·70 | 12·80 | 1·000 | 0·003 | 0·878 | 0·003 | 0·826 | 0·005 | 0·941 | 0·003 | 0·823 | 0·004 | 0·938 | 0·004 |
| Ischia | I 2SF | 5·7 ± 1·8 | 0·705053 | ±6 | 0·512683 | ±6 | 2·58 | 7·79 | 1·002 | 0·004 | 1·005 | 0·003 | 0·873 | 0·006 | 0·869 | 0·004 | 0·866 | 0·005 | 0·862 | 0·004 |
| Ischia | I 109 | 22·8 ± 5·2 | 0·706122 | ±6 | 0·512598 | ±5 | — | — | — | — | — | — | — | — | — | — | — | — | — | — |
| Procida | FAM 10 | 55 ± 5 | 0·706556 | ±9 | 0·512536 | ±6 | 2·62 | 9·27 | 1·004 | 0·004 | 0·858 | 0·003 | 0·848 | 0·006 | 0·987 | 0·004 | 0·841 | 0·005 | 0·979 | 0·006 |
| Procida | FAM 10 *rep* | 55 ± 5 | — | — | — | — | | | — | — | — | — | 0·856 | 0·007 | — | — | 0·857 | 0·006 | — | — |
| Procida | UPFUC | 21·30 ± 0·17 | 0·707329 | ±8 | 0·512471 | ±6 | 3·80 | 11·89 | 1·002 | 0·002 | 0·970 | 0·003 | 0·913 | 0·005 | 0·941 | 0·003 | 0·901 | 0·004 | 0·928 | 0·003 |
| *RMP—northern districts* | | | | | | | | | | | | | | | | | | | | |
| Latera | Bols 301 | 158 ± 5 | *0·709930*[1] | — | *0·512185*[1] | — | 8·06 | 50·36 | 0·985 | 0·005 | 0·485 | 0·002 | 0·567 | 0·004 | 1·169 | 0·005 | — | — | altered | — |
| Latera | Bols 301 *rep* | 158 ± 5 | — | — | — | — | 8·66 | 53·42 | 0·982 | 0·003 | 0·492 | 0·002 | 0·565 | 0·003 | 1·147 | 0·004 | — | — | altered | — |

(continued)

*Table 3: Continued*

| Province, volcano | Sample | Age (ka) | $^{87}Sr/^{86}Sr$ | 2 σm | $^{143}Nd/^{144}Nd$ | 2 σm | U (ppm) | Th (ppm) | $(^{234}U/^{238}U)$ | 2 σm | $(^{238}U/^{232}Th)$ | 2 σm | Measured values | | | | Age-corrected values | | | |
|---|---|---|---|---|---|---|---|---|---|---|---|---|---|---|---|---|---|---|---|---|
| | | | | | | | | | | | | | $(^{230}Th/^{232}Th)_m$ | 2 σm | $(^{230}Th/^{238}U)_m$ | 2 σm | $(^{230}Th/^{232}Th)_i$ | 2 σm | $(^{230}Th/^{238}U)_i$ | 2 σm |
| Vico | VCO 20 | 120 ± 6 | *0·708351*[2] | — | *0·512234*[2] | — | 6·92 | 28·99 | 0·999 | 0·004 | 0·725 | 0·003 | 0·727 | 0·004 | 1·002 | 0·004 | 0·730 | 0·008 | 1·007 | 0·012 |
| Vico | VCO 3 | 120 ± 6 | *0·708124*[2] | — | *0·51223*[2] | — | 6·47 | 26·54 | 0·993 | 0·004 | 0·740 | 0·003 | 0·734 | 0·005 | 0·992 | 0·004 | 0·722 | 0·008 | 0·975 | 0·011 |
| Middle Latin Valley | S 18 | 80 ± 40 | *0·709743*[1] | — | *0·512121*[1] | — | 6·40 | 28·07 | 0·994 | 0·003 | 0·692 | 0·003 | 0·701 | 0·005 | 1·014 | 0·004 | 0·714 | 0·011 | 1·031 | 0·015 |
| Middle Latin Valley | S 18 *rep* | 80 ± 40 | — | — | — | — | — | — | — | — | — | — | 0·699 | 0·004 | — | — | 0·708 | 0·008 | 1·023 | 0·012 |
| Latera | Bols 282 | 180 ± 7 | *0·710310*[1] | — | *0·512114*[1] | — | 7·61 | 31·39 | 1·003 | 0·004 | 0·737 | 0·003 | 0·740 | 0·005 | 1·004 | 0·004 | 0·753 | 0·014 | 1·022 | 0·020 |
| Middle Latin Valley | S 9 | 180 ± 90 | *0·706642*[1] | — | — | — | 2·97 | 9·41 | 0·997 | 0·004 | 0·959 | 0·004 | 0·966 | 0·005 | 1·007 | 0·004 | 0·995 | 0·037 | 1·038 | 0·039 |
| Middle Latin Valley | S 9 *rep* | 180 ± 90 | — | — | — | — | 3·00 | 9·37 | 0·992 | 0·005 | 0·972 | 0·013 | 0·967 | 0·005 | 0·994 | 0·004 | 0·943 | 0·035 | 0·970 | 0·038 |
| Montefiascone | VS 189 | 245·3 ± 4·7 | *0·710272*[1] | — | *0·512053*[1] | — | 12·65 | 48·44 | 1·002 | 0·005 | 0·793 | 0·004 | 0·793 | 0·005 | 1·000 | 0·004 | 0·790 | 0·031 | 0·997 | 0·042 |
| Alban Hills | VLS 02 | 277 ± 2 | 0·710342 | ±7 | 0·512103 | ±5 | 6·19 | 52·46 | 0·985 | 0·004 | 0·358 | 0·000 | 0·409 | 0·003 | 1·140 | 0·004 | — | — | altered | — |
| Alban Hills | VLS 35 | 278 ± 5 | 0·710279 | ±6 | 0·512099 | ±5 | 8·45 | 36·71 | 0·992 | 0·003 | 0·700 | 0·003 | 0·703 | 0·004 | 1·004 | 0·004 | 0·740 | 0·036 | 1·057 | 0·057 |
| Alban Hills | VLS 43 | 278 ± 5 | 0·710176 | ±6 | 0·512100 | ±4 | — | — | — | — | — | — | — | — | — | — | — | — | — | — |
| Alban Hills | VLS 12 | 277 ± 2 | 0·710377 | ±7 | 0·512098 | ±5 | 11·18 | 57·10 | 0·998 | 0·004 | 0·595 | 0·002 | 0·599 | 0·003 | 1·006 | 0·004 | 0·642 | 0·028 | 1·078 | 0·051 |
| Alban Hills | VLS 25 | 287 ± 6 | 0·710291 | ±7 | 0·512102 | ±5 | 13·32 | 50·15 | 1·004 | 0·004 | 0·806 | 0·005 | 0·803 | 0·005 | 0·996 | 0·004 | 0·765 | 0·048 | 0·949 | 0·077 |
| Bolsena | VS 67 | 256 ± 3 | *0·710190*[1] | — | *0·512094*[1] | — | 5·64 | 28·90 | 0·993 | 0·005 | 0·593 | 0·003 | 0·595 | 0·005 | 1·003 | 0·005 | 0·612 | 0·028 | 1·031 | 0·049 |
| *TMP* | | | | | | | | | | | | | | | | | | | | |
| Amiata | AMT 20 | 209 ± 29 | *0·710889*[1] | — | *0·512157*[1] | — | — | — | — | — | — | — | — | — | — | — | — | — | — | — |
| Amiata | AMT 82 | 209 ± 29 | 0·711613 | ±8 | 0·512093 | ±5 | 9·32 | 38·21 | 0·995 | 0·003 | 0·740 | 0·003 | 0·749 | 0·005 | 1·013 | 0·004 | 0·806 | 0·028 | 1·089 | 0·036 |
| Amiata | AMT 44 | 203 ± 12 | 0·712110 | ±5 | 0·512096 | ±5 | 9·97 | 39·47 | 1·003 | 0·004 | 0·766 | 0·003 | 0·771 | 0·005 | 1·006 | 0·004 | 0·795 | 0·020 | 1·038 | 0·027 |
| Amiata | AMT 38 | 203 ± 12 | 0·712639 | ±5 | 0·512095 | ±7 | 8·78 | 37·77 | 0·998 | 0·004 | 0·707 | 0·003 | 0·712 | 0·005 | 1·007 | 0·003 | 0·740 | 0·016 | 1·047 | 0·026 |

Data sources: [1]Conticelli *et al*. (2002); [2]Perini *et al*. (2004); *rep* indicates replicate analyses. Parentheses denote activity; Subscripts m and i stand for measured and initial value, respectively; 2 σm is the standard error on the mean and for Sr and Nd isotopes refers to the last digit.

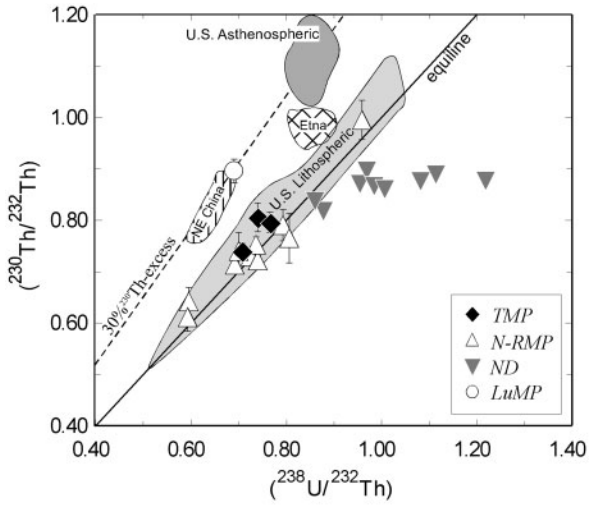


**Fig. 5.** ($^{230}$Th/$^{232}$Th) vs ($^{238}$U/$^{232}$Th) equiline diagram. Parentheses indicate activity ratios. All activity ratios are age-corrected (i.e. initial). When error bars are not shown, the error is smaller than the symbol size. Fields for within-plate continental alkalic volcanic rocks reported for comparison include: Etna, Condomines *et al.* (1995); NE China, Zou *et al.* (2003); US lithospheric, Asmerom & Edwards (1995), Reid (1995), Reid & Ramos (1996), Asmerom (1999) and Asmerom *et al.* (2000); US asthenospheric, Asmerom & Edwards (1995), Asmerom (1999) and Asmerom *et al.* (2000).

## U–Th disequilibria

This study specifically focuses on the youngest, least evolved magmatic rocks of each sector of the Italian volcanic province. Unfortunately, the ages of many of the samples (i.e. 150–300 ka; see Tables 1 and 3) make them less than ideal for U-series work; however, in many cases, they represent the only samples available within the time window for U-series disequilibrium study. Although the age-related uncertainties on the U–Th measurements of these rocks make them unsuitable for detailed investigation of melting models, such data still provide significant constraints on the processes of mantle metasomatism and mantle mineralogy in the various magmatic sectors. Limiting our U–Th analyses only to the youngest products, which require minimal age correction (i.e. ND), would have precluded obtaining a fuller picture of the Italian magmatism, which is characterized by strong geographical- and age-related variations.

The $^{238}$U–$^{230}$Th disequilibrium of old samples is perturbed not only by return to equilibrium but also, potentially, by the effects of weathering. Alteration by surficial water can induce significant preferential leaching of U, which is more fluid-mobile in oxidizing conditions than Th (Rosholt & Noble, 1969; Rosholt *et al.*, 1973; Cohen *et al.*, 1996), and this will elevate ($^{230}$Th/$^{238}$U) activity ratios (all ratios reported inside parentheses are activity ratios). However, such weathering should also affect ($^{234}$U/$^{238}$U) as a result of the preferential leaching of $^{234}$U relative to $^{238}$U [see reviews by Ivanovich & Harmon (1992) and Porcelli & Swarzensky (2003)]. To avoid any significant influence of secondary alteration on our samples, we therefore exclude from further discussion samples with ($^{234}$U/$^{238}$U) outside error of equilibrium (see the Appendix).

$^{238}$U–$^{230}$Th disequilibria in the selected samples are shown in the classic equiline diagram of Fig. 5. All activity ratios reported in the diagrams and those referred to in the text are age-corrected (i.e. initial) unless otherwise stated. The equiline diagram illustrates the three styles of behaviour in the studied samples: (1) ND rocks display ubiquitous $^{238}$U excesses up to values of ~30%; (2) TMP and N-RMP rocks lie close to the equiline; (3) the sole LuMP sample that does not show obvious secondary alteration has a clear ~30% $^{230}$Th excess.

The measured (i.e. not age-corrected) $(^{230}\mathrm{Th}/^{238}\mathrm{U})_m$ for the TMP and N-RMP samples cluster close to equilibrium, between 0·992 and 1·014. The sometimes large age corrections widen the range of possible initial ($^{230}$Th/$^{238}$U) disequilibria from 0·949 to 1·089 (Table 3). The uncertainties of the age determinations have been taken into account in the reported propagated errors (see the Appendix; and as shown by error bars in Fig. 5) and can substantially increase the errors in initial ($^{230}$Th/$^{238}$U) (e.g. samples S9 and S18; Tables 1 and 3). Focusing attention only on some of the younger products, such as those from Vico and the Middle Latin Valley (Table 3), the range of age-corrected values shrinks even closer to secular equilibrium (0·975–1·031). U–Th isotopic compositions near secular equilibrium are also reported for differentiated lavas and pyroclastic flows from Vico (Villemant & Flehoc, 1989) and the Alban Hills (Voltaggio *et al.*, 1994); the latter show eruption ages <33 ka determined by an internal $^{230}$Th–$^{238}$U isochron method. From all these observations, we suggest that the near-equilibrium compositions reported for the older samples are also an original characteristic of these rocks and are not a consequence of time-dependent return to secular equilibrium.

Regardless of the almost constant equilibrium composition for $^{238}$U–$^{230}$Th, the samples from TMP and N-RMP display variable ($^{230}$Th/$^{232}$Th), ranging from 0·61 to 0·80, with the only exception being the shoshonite from the Middle Latin Valley, which has a distinctly higher values (0·94). On the other hand, ($^{230}$Th/$^{232}$Th) is near constant in the rocks from the ND, which instead have variable ($^{230}$Th/$^{238}$U) from 0·728 to 0·979, with the highest excesses in the samples from Vesuvius.

The three samples of LuMP have measured $(^{230}\mathrm{Th}/^{238}\mathrm{U})_m$ >1 (Table 3). As described above, these samples are mafic lapilli, which have been mechanically treated to exclude secondary alteration. However, two of the measured samples (VLT 37 and VLT 92) had to be discarded on the basis of their low ($^{234}$U/$^{238}$U). The sole

remaining sample (VLT 99) shows 30% initial $^{230}Th$ excess and a ($^{234}U/^{238}U$) value close to equilibrium, although formally outside error of unity, based on the reproducibility of our TML replicates (see the Appendix). Other ($^{234}U/^{238}U$) values just outside error of unity have been measured in a few N-RMP samples (i.e. VCO 3, S 9, VLS 35), but these samples display near-equilibrium ($^{230}Th/^{238}U$), similar to the samples with ($^{234}U/^{238}U$) clearly in equilibrium. Therefore, we interpret the elevated ($^{230}Th/^{238}U$) in VLT 99 as dominantly a primary, melt-induced signature. As a further test of the reliability of this measurement, we compared the elemental U/Th of the three LuMP samples with those of the petrographically fresher but older lavas (Table 2), which were not suitable for U–Th isotope measurement. The U/Th of VLT 99 is the same as those of older unaltered lavas (~0·20), and distinctly higher than those of the two discarded samples (~0·15). This supports our notion that the ($^{230}Th/^{238}U$) of VLT 99 can be used reliably to investigate the melting process involved in the generation of LuMP lavas.

## DISCUSSION

It has been shown that the strong incompatible element enrichment of the Italian ultrapotassic mafic volcanic rocks, along with their enriched Sr–Nd isotopic signature, requires the involvement of recycled crustal material in their petrogenesis, either imprinted in the mantle source by subduction (Peccerillo, 1985; Conticelli & Peccerillo, 1992; Hawkesworth *et al.*, 1993), or acquired during magma ascent to the surface by crustal assimilation (Gasperini *et al.*, 2002). On the other hand, secular isolation of a lithospheric mantle source might also produce extremely enriched Sr–Nd isotopic compositions, but is unable to drive Pb and Os isotopic ratios to typical crustal compositions (e.g. Conticelli *et al.*, 2002, 2007), or typically account for the highly fractionated LILE/HFSE observed in the ultrapotassic rocks (Peccerillo, 1985; Rogers *et al.*, 1985).

### Influence of crustal contamination and magmatic differentiation

The implausibility of generating the extreme enrichment of these lavas by crustal assimilation has been thoroughly discussed in previous studies (e.g. Conticelli, 1998; Conticelli *et al.*, 2007). In general terms, a significant role for crustal contamination is inconsistent with the strongly silica-undersaturated character of the magmas. The extreme enrichments in incompatible trace elements are more in keeping with small degrees of mantle melting (especially with high $CO_2$) rather than major additions of siliceous anatectic melts. Carbonate assimilation might not drive contaminated magmas to oversaturated compositions, but would impart them with a striking trace element signature that is not observed (e.g. strong enrichments in Sr and high U/Th). Finally the strong HREE fractionation is neither a feature of possible contaminating crust nor a result of plausible fractionating phases. Given that the elevated incompatible element abundances are thus primary, the subsequent influence of modest amounts of crustal contamination is then limited.

Within individual magmatic suites, Bohrson & Spera (2001) demonstrated that energy-constrained assimilation–fractional crystallization (EC-AFC) processes do not always produce monotonic variation of isotope ratios (i.e. Sr and Nd) with indices of differentiation (i.e. incompatible trace element abundance or silica content), and that more complex patterns may result from the differences in the trace element concentrations of the original magma and the anatectic melt, and the more or less compatible behaviour of these elements during mantle melting. However, in the case of 'basaltic' compositions, crustal assimilation should be linked to the crystallization of mafic phases and therefore to a decrease in the MgO content of the melt. This implies that strongly contaminated melts should have low MgO. This can be tested using our most comprehensively sampled, cogenetic lava suites from the Alban Hills and Vesuvius. These datasets show a wide range of MgO contents for both suites (5·2–8·2 wt % and 3·0–7·5 wt %, respectively) at almost constant $^{87}Sr/^{86}Sr$ (Table 3), leaving little scope for the role of contamination on incompatible element budgets. Only the Monte Amiata (TMP) rocks show any sense of an inverse relationship between $^{87}Sr/^{86}Sr$ and MgO that might be suggestive of crustal contamination.

More specifically, the effect of crustal contamination on the U–Th isotope compositions depends on whether the process of wall-rock anatexis is able to fractionate U from Th or not. The magnitude and direction of this fractionation is difficult to estimate given the lack of knowledge of the mineralogy and melting relationships of the possible wall-rock contaminants. Studies on magma suites showing clear AFC trends (Nicholson *et al.*, 1991) have illustrated that old basaltic crust can be assimilated with little fractionation of U and Th. Recently, Berlo *et al.* (2004) demonstrated that partial melting of the lower crust is only able to produce small degrees of disequilibrium in the anatectic melts and suggested that crustal contamination has little influence on the U-series disequilibria measured in arc lavas. In our dataset, the only samples showing possible evidence of crustal contamination, those from the TMP, have ($^{230}Th/^{238}U$) slightly higher than the high-MgO rocks of the N-RMP.

The effect of crustal contamination might be different on ND rocks, because the volcanoes of this area are emplaced on a thick sequence of Mesozoic limestone, highly enriched in U with respect to Th (Del Moro *et al.*, 2001). Bohrson *et al.* (2006) have suggested that crustal

contamination can explain the negative slope on the equiline diagram defined by U–Th isotope variation in pumice samples from the Campanian Ignimbrite (ND). Bohrson *et al.* did not indicate the direction of the crustal contamination effect, but assuming a carbonate wall-rock contaminant with a high U/Th ratio, and thus high ($^{230}Th/^{232}Th$), their data imply that crustal contamination in the Neapolitan area would drive the composition of the magmas towards higher ($^{230}Th/^{238}U$). This cannot account for the $^{238}U$ excess measured in the much less evolved samples in this study. This conclusion is also supported by a detailed study of the effect of wall-rock contamination on the magmas of the 1944 eruption of Vesuvius (Del Moro *et al.*, 2001), which demonstrated that contamination is extremely limited and concentrated in a skarn layer, which effectively insulates the magma chamber.

Thus, neither within the overall chemical characteristics nor in the trends of individual volcanic suites do we see a potentially significant role for crustal contamination in the studied rocks, except perhaps for the TMP lavas. The complexity of contamination processes (Bohrson & Spera, 2001; Spera & Bohrson, 2001), however, makes it difficult to discount the role of any contamination. Indeed, it is not unlikely that some of our samples have assimilated minor amounts of crust, but this does not affect the broad chemical and isotopic characteristics that we are investigating.

In interpreting trace element signatures, fractional crystallization, in addition to crustal assimilation, must also be considered, especially for the samples with low MgO contents, such as those from the TMP and ND. Although we characterize these rocks using highly incompatible trace element ratios, which should remain only modestly influenced by removal of the major crystallizing phases, the fractionation of accessory phases such as leucite or apatite could account for some of the observed geochemical characteristics, such as the negative Ba and P anomalies shown in Fig. 3. However, Ba depletion is independent of both the degree of silica saturation (i.e. leucite crystallization) of the magmas (e.g. TMP vs N-RMP) and their degree of evolution (i.e. MgO content), but instead appears to vary on a geographical basis. As a clear example, strong Ba anomalies are present in the silica-saturated TMP rocks (Fig. 3), where leucite is not a crystallizing phase (Table 1), but not in the leucite-bearing silica-undersaturated HKS rocks of the ND. In Fig. 2, the MgO and $P_2O_5$ contents of the studied rocks are plotted along with previously published data for the Italian magmatic provinces to show the overall liquid lines of descent and to determine the onset of apatite fractionation. All the N-RMP and LuMP samples have MgO contents too high to be affected by apatite fractionation. Some of the TMP and ND samples with lower MgO contents might have experienced apatite fractionation. However, there are no negative P anomalies in the ND samples, whereas the negative P anomalies in the TMP samples are not restricted to those with low MgO (Fig. 3).

Apatite or leucite fractionation could also have affected the primary U–Th isotope composition of the erupted magmas. U–Th isotope data on leucite and apatite mineral separates from the Alban Hills (N-RMP, Voltaggio *et al.*, 1994) and Vesuvius (ND, Black *et al.*, 1998) volcanic rocks indicate $^{238}U$ and $^{230}Th$ excesses, respectively. The low partition coefficients and absolute abundances of Th and U in leucite (Voltaggio *et al.*, 1994) make its assimilation or fractionation unlikely to have had a significant effect on the U–Th disequilibria of the erupted magmas. On the contrary, apatite fractionation could strongly affect U–Th disequilibria as a result of its enrichment in Th (and to a lesser extent U). It is significant, however, that $^{238}U$ excesses have been measured only in ND rocks where apatite does not occur petrographically (Table 1) and P depletion is not present. Moreover, apatite removal (or accumulation) would result in a correlation between U–Th disequilibria and P contents, which is not observed either in TMP and N-RMP rocks, or in ND rocks.

Therefore we conclude that the geochemical and isotopic signatures reported for the studied samples have to be related to processes affecting the sources of these magmas, and are linked to the past or present-day occurrence of subduction beneath the Italian peninsula.

## Source enrichment

The different mobility of incompatible elements in a fluid phase has long been considered the principal cause of LILE/HFSE fractionation and $^{238}U$ excesses in sediment-poor arc lavas (Hawkesworth *et al.*, 1997). Strong fractionations between LILE and HFSE have also been observed in island arcs where the budget of incompatible trace elements is clearly dominated by sediment addition (e.g. Sunda arc, Whitford *et al.*, 1979; Hoogewerff *et al.*, 1997; Banda, Vroon *et al.*, 1993); this feature can be attributed either to the original LILE/HFSE fractionation in the sedimentary end-members (Plank & Langmuir, 1998) or to the presence of a residual phase retaining HFSE (Ta, Nb, Hf, Zr and Ti) during sediment melting (Nichols *et al.*, 1994; Elliott *et al.*, 1997; Johnson & Plank, 1999). Particularly interesting is the behaviour of Th, which is not partitioned into slab-derived fluids, but can be efficiently transferred from the subducted sediments into the mantle wedge via partial melts (Johnson & Plank, 1999). These observations have led to the suggestion that high Ba/Th and U/Th ratios are indicative of a fluid-dominated subduction component, whereas high Th, Th/Nb and Th/REE ratios are distinctive of greater recycled sediment contributions (Elliott *et al.*, 1997; Hawkesworth *et al.*, 1997; Class *et al.*, 2000; Plank, 2005). The extremely high Th

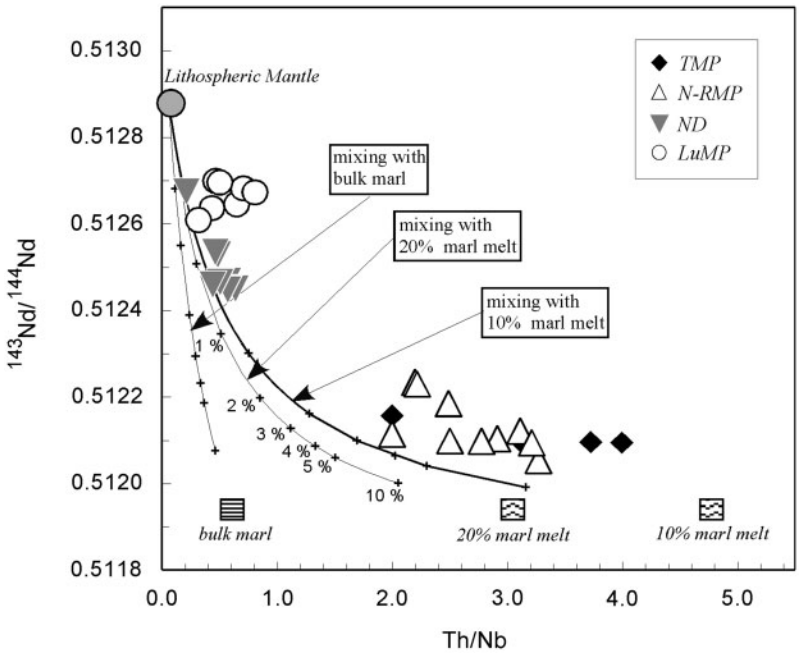


**Fig. 6.** $^{143}Nd/^{144}Nd$ vs Th/Nb. Mixing lines between the lithospheric mantle and the three potential sediment-derived enriching agents as in Fig. 4 are also shown. End-member compositions and bulk partition coefficients for sediment melting are evaluated as in Fig. 4. The values adopted in the calculation are as follows: mantle end-member: Nd 0·4 ppm, Th 0·03 ppm, Nb 0·5 ppm; bulk sediment end-member: Nd 21·4 ppm, Th 7·25 ppm, Nb 11·8 ppm; partition coefficients for sediment melting: $D_{Th} = 0{\cdot}08$, $D_{Nb} = 1{\cdot}43$, $D_{Nd} = 0{\cdot}26$. Curves are drawn between zero and 10% sediment (or sediment melt) addition and the tick marks represent the same amount of sediment addition as in Fig. 4 (i.e. 0·5%, 1%, 2%, 3%, 4%, 5% and 10%). The composition of the sediment end-members is also shown. Sediment melting is necessary to explain the high Th/Nb of the observed rocks, and the ratio in the sediment melts (or supercritical liquids) is mostly controlled by the amount of residual rutile. A value of 0·26% rutile is used in the calculation (Kessel *et al.*, 2005), but higher amounts of residual rutile would generate sediment melts with higher Th/Nb. A further increase in the Th/Nb ratio (not shown in the diagram) could result from the melting of the metasomatized mantle source. However, because of the generally similar behaviour of Th and Nb during mantle melting [e.g. see partition coefficients from Workman & Hart (2005)] the enrichment factor $[(Th/Nb)_{melt}/(Th/Nb)_{source}]$ cannot exceed 1·3 for degrees of melting $f > 0{\cdot}5\%$.

contents and Th/Nb (Fig. 6) of the Italian volcanic rocks suggest that their geochemical characteristics could not have been produced simply by fluid addition to the mantle wedge. In further support of a sedimentary component, increasing Th/Nb is associated with a trend towards low $^{143}Nd/^{144}Nd$ typical of local Italian sediments (Fig. 6).

Unfortunately, constraining an exact composition of the sediments responsible for the enrichment of the mantle is not straightforward in the case of the Italian magmatism. In part, this is due to the complex geodynamic evolution of the area. Because the Apennine margin is at present the site of continental collision, any sediments deposited in the Tethyan basin will have been subducted along with the Adriatic slab, and therefore cannot be directly sampled. However, the Apennine chain is believed to be built from the sedimentary successions, mainly an alternation of clay-rich and carbonate sediments, which were deposited in the Tethyan basin and have been subsequently off-scraped onto the continental margin (e.g. Treves, 1984). Therefore, the sedimentary succession cropping out along the Apennine orogen can be used to constrain the likely composition of the subducted sediment. The primordial mantle-normalized trace element patterns of some Italian end-member sediments are reported in Fig. 7. The Ba (and P) negative anomalies in the Italian sediments well match those displayed by the rocks of the TMP and N-RMP (Fig. 3), suggesting that these geochemical characteristics of the volcanic rocks might be inherited from those of the recycled sedimentary component.

To place more quantitative constraints on the source enrichment process we have attempted to reproduce the observed data, modelling the process of mantle metasomatism by addition of both bulk sediment and sediment melt components (see captions of Figs 4 and 6 for further details). The mantle end-member composition was estimated on the basis of a selected number of relevant European peridotite massifs (Downes, 2001). For the sediment end-member, we assumed a 50:50 mix of Italian clay-rich (Melluso *et al.*, 2003; Mongelli & Dinelli, 2001) and carbonate sediments (Del Moro *et al.*, 2001), identified as marl in Fig. 7. Trace element partition coefficients were taken from the values measured by Kessel *et al.* (2005) at 6 GPa and 800 C for melts in equilibrium with a

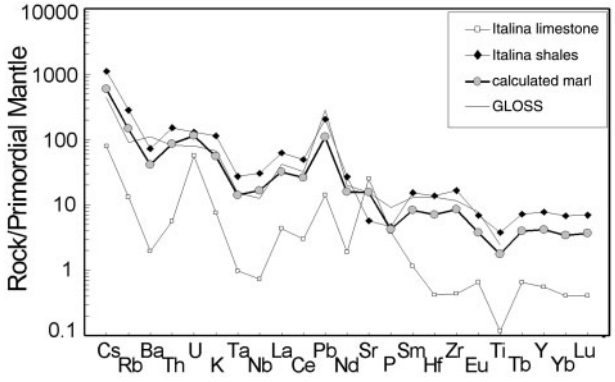


**Fig. 7.** Incompatible trace element patterns normalized to the primordial mantle (Sun & McDonough, 1989) for indicative Italian carbonate-rich sediments (limestone from Vesuvius: Del Moro *et al.*, 2001) and clay-rich sediments (Ligurides shales: Mongelli & Dinelli, 2001) representing possible end-member compositions of the subducted sediment assemblage: the composition of the estimated marl used in the model (Figs 4 and 5) is also shown along with that of the Global Subducted Sediments (GLOSS: Plank & Langmuir, 1998). Italian sediments have negative Ba anomalies, not present in GLOSS, which are strikingly similar to those shown in Fig. 3 by the TMP and N-RMP samples.

basaltic composition. The rationale for this choice is because at a pressure >4 GPa sediments and basalts have the same eclogitic mineralogy (although different mineral proportions), except for the occurrence of phengite (Schmidt *et al.*, 2004) and possibly carbonate phases (Kerrick & Connolly, 2001). Because phengite is rapidly removed from the residual sediment (Schmidt *et al.*, 2004) the bulk partition coefficients measured for basalts can be equally applied to the sediments, provided the different mineral proportions are taken into account. Indeed, the higher proportion of coesite and kyanite in the residual sediment (~50%, Schmidt *et al.*, 2004) than in basalt requires that the bulk solid/liquid partition coefficients of the sedimentary component be roughly reduced by a factor of 0·5 with respect to those measured in basalt (see also Tommasini *et al.*, 2007).

The model is necessarily a great simplification of more complex processes and does not take into consideration the regional variation that is likely to occur in the compositions both of the mantle and the subducting sediments along the study region. Nevertheless, we think it provides some insights into the sediment recycling process.

The results of our model are displayed in Figs 4 and 6. Mantle metasomatism with <5 wt % of sediment-derived melt is able to reproduce the Sr–Nd isotope compositions of all the studied samples, except for those from the TMP, which require an end-member with more radiogenic $^{87}Sr/^{86}Sr$, probably representing a higher clay to carbonate proportion in the subducting sediment component. Also, the higher Th/Nb of the TMP samples can be modelled by considering a higher amount of residual rutile during sediment melting, again consistent with higher clay to carbonate proportion. The amount of rutile is a poorly constrained parameter and so we have not tried to precisely reproduce lava compositions in Fig. 6, but only show the plausibility of the general concept.

## $^{238}U$ excess: the Neapolitan District

Vesuvius lavas with $(^{230}Th/^{238}U)$ <1 were first reported in the pioneering work of Capaldi *et al.* (1982) and more recently by Cortini *et al.* (2004) and Voltaggio *et al.* (2004). Having excluded, in the discussion above, the possibility of generating $^{238}U$ excesses by crustal assimilation, addition of a distinct, recent, U-rich component to the already sediment-metasomatized mantle wedge is required. This has important consequences for the interpretation of the genesis of ND magmas, as it strongly implies that these lavas result from subduction processes.

The significant $^{238}U$ excesses measured in the high-Th Neapolitan rocks is atypical of arc-lavas worldwide (Fig. 8a and b). Previously, Kick'em Jenny in the Lesser Antilles (Gill & Williams, 1990: Turner *et al.*, 1996) was the sole oceanic exception to the rule of significant $^{238}U$ excesses only in the most depleted lavas. The Vesuvius case is yet more extreme. The ND rocks define a trend of increasing $(^{238}U/^{230}Th)$ with decreasing Th concentration, as is the case for arc lavas in general, which is consistent with a given amount of U enrichment being most apparent in the least incompatible element enriched sources. At Vesuvius, however, the total amount of added U, via metasomatism, has to be anomalously high with respect to typical island arcs. The addition of subduction-related fluids has been argued to be responsible for the observed disequilibria in Vesuvius by Voltaggio *et al.* (2004) and Cortini *et al.* (2004), and has been claimed also by Schiano *et al.* (2004) to explain the strong enrichment of fluid mobile elements, such as Ba and Rb, in olivine-hosted melt inclusions in Vesuvius lavas. The higher Ba/Th ratios measured in the ND rocks (Fig. 8b), with respect to those from all the other studied samples is consistent with a Ba-rich component affecting only the Neapolitan region. However, the measured Ba/Th ratios of the studied Vesuvius samples are still low in comparison with typical island arcs with high $^{238}U$ excesses (Fig. 8b) and define an almost vertical trend of increasing $(^{238}U/^{230}Th)$ at near-constant Ba/Th. This suggests either two different added components or a single component with variable Ba/U.

The almost horizontal trajectory of U enrichment in the equiline diagram (Fig. 5) requires a U addition process shortly before magma genesis (taking the slope at face value as an isochron). Therefore, the U-enriched component is likely to originate from a source different from that responsible for the overall sediment-related metasomatism that affects the Italian region as a whole.

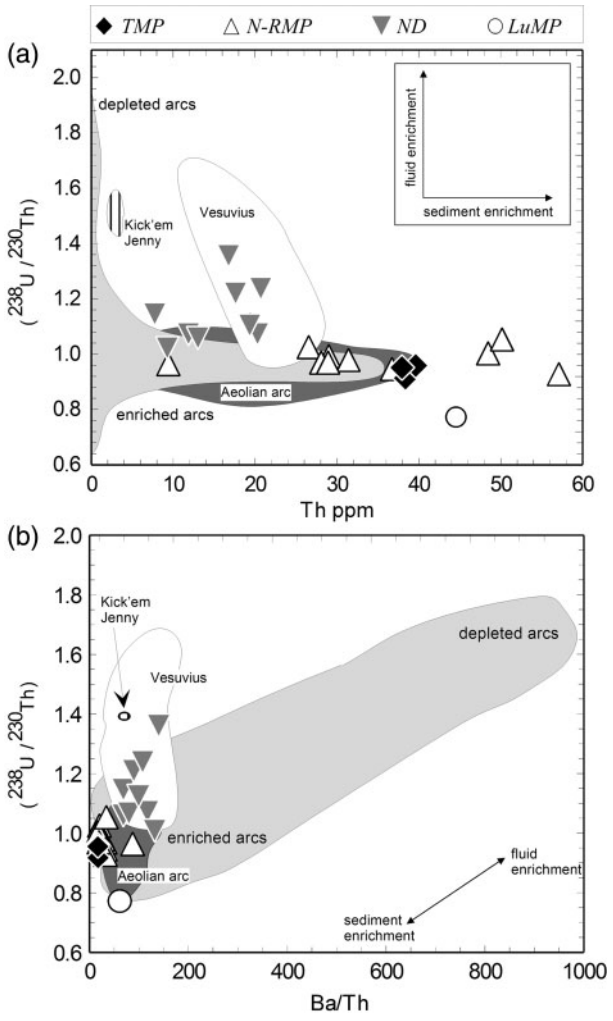


**Fig. 8.** (a) ($^{238}U/^{230}Th$) vs Th ppm for the Italian rocks of this study along with published data from Vesuvius (white field), and worldwide island arc lavas (light grey field). Published data for rocks from the Aeolian Islands (dark grey field; Francalanci *et al.*, 2007) are also reported as representative of island arc lavas erupted in the same geographical region. All the samples in this study plot along the trend of 'sediment-dominated' enriched arcs (e.g. Hawkesworth *et al.*, 1997) and have Th concentrations among the highest measured for subduction-related rocks. The $^{238}U$ excesses measured in the ND samples lie outside the field of typical island arc rocks, requiring an anomalously high amount of U to be added to their mantle source. (b) ($^{238}U/^{230}Th$) vs Ba/Th. The literature fields are the same as in (a). ND rocks have higher Ba/Th than the other studied samples, but define an almost vertical trend of $^{238}U$ excesses at near-constant Ba/Th, outside the main trend of island arc magmas. A position similar to that of the ND samples has been reported for Kick'em Jenny in the Lesser Antilles (Gill & Williams, 1990; Turner *et al.*, 1996).

The presence of still-active oceanic subduction of the Ionian plate beneath Calabria (Fig. 1) is the most likely candidate. According to seismic and tomographic studies (Selvaggi & Chiarabba, 1995; Piromallo & Morelli, 2003), the Ionian slab lies at much greater depth beneath the Neapolitan area (>350 km) than in typical arcs.

Uncertainty remains regarding the nature of the U enrichment. As outlined above, slab-derived fluids appear to influence only the U budget of incompatible element-depleted mantle sources. A typical slab-derived fluid component thus seems unlikely to significantly affect the high Th and U source of the ND rocks. On the other hand, sediment-derived melts are able to carry higher amounts of incompatible trace elements. However, the sense and magnitude of U fractionation from Th during sediment melting is still poorly known and likely to be variable. U-enriched sediment melts have been suggested by Elliott *et al.* (1997) to explain the isotopic composition of the Marianas arc. On the contrary, experimental studies on sediment melting have demonstrated that melting of clay-rich sediment at sub-arc depths (2–6 GPa) generates Th-enriched melts (Johnson & Plank, 1999; Kessel *et al.*, 2005).

In our opinion the great depth of the Benioff Zone beneath the Neapolitan area, along with the presence of carbonate-rich sediments on the subducting Ionian slab (Krom *et al.*, 1999; Weldeab *et al.*, 2002), both of which are anomalous in a global view of arc magmatism, could represent the key factors in generating the unusual U excesses at Vesuvius. At high pressures, separate melts and fluid phases are replaced by a single supercritical liquid, and above the second critical end-point of the solidus, the amount of solute and the solubility of $H_2O$ both increase in this supercritical liquid (Hermann *et al.*, 2006, and references therein). Unfortunately, few constraints on the trace element composition of supercritical liquids from carbonate-rich sediments are available. However, the propensity of U to complex with carbonate ions, as indicated by the extreme $^{238}U$ excesses measured in carbonatitic magmas (Williams *et al.*, 1986; Pyle *et al.*, 1991) might suggest that a carbonate-rich liquid would be a favourable environment for U relative to Th. Carbonates are believed to behave as refractory phases at sub-arc depths (up to 180 km: Yaxley & Green 1994; Molina & Poli, 2000; Schmidt *et al.*, 2004). Kerrick & Connolly (2001) have demonstrated that carbonate–clay-rich sediments (i.e. marls) de-volatilize and de-carbonate at sub-arc conditions only if the sediment pile is flushed by a large amount of water, such as that liberated at high pressure from the underlying subducted peridotitic mantle (e.g. Rüpke *et al.*, 2004). It is, therefore, tempting to speculate that a high-pressure $H_2O$-rich supercritical fluid could become enriched in U over Th during interaction with neighbouring carbonates. The lack of relevant experimental studies on carbonate-rich sediments at high-pressure conditions precludes more rigorous exploration of the mechanism of U enrichment, but we feel that the circumstantial evidence of deep carbonate subduction favours a mechanism along the lines of that tentatively suggested above.

## U–Th secular equilibrium: TMP and N-RMP rocks

Although TMP and N-RMP sources require considerable enrichment by addition of recycled sediments, active subduction under this area ceased at 21–16 Ma (Faccenna *et al.*, 2001). Thus, any U–Th disequilibrium should be related to the most recent tectonic events that have led to source melting and magmatism, rather than to subduction processes. The mechanism that triggers melting in the northernmost Italian area is still debated. Two main processes have been invoked: (1) lithospheric-scale stretching after the cessation of subduction of the Adriatic lithosphere and back-arc asthenospheric mantle up-doming (e.g. Savelli, 2000, and references therein); (2) intra-continental rifting unrelated to subduction (e.g. Stoppa & Lavecchia, 1992, and references therein). The possibility of melting related to a lithospheric stretching extensional regime is also supported by the high heat flow (Della Vedova *et al.*, 1984), reduced lithospheric thickness (~70 km, Peccerillo & Panza, 1999), and anomalously high seismic wave attenuation (Mele *et al.*, 1996) found beneath the Apennine chain and on its Tyrrhenian margin side. Whatever the model, the mantle melting process itself must be regarded as a post-collision intra-continental melting event

Within-plate magmatism results in melts with U–Th disequilibria that range from near equilibrium to strong $^{230}$Th excesses [for a thorough review, see Bourdon & Sims (2003)]. Asmerom (1999) investigated the U–Th disequilibria in various intra-continental, rift-related magmatic associations from the southern USA and Mexico, which span much of the range in disequilibrium for within-plate continental magmas as a whole. He reported near-equilibrium U–Th compositions for lithosphere-derived magmas and significant $^{230}$Th excesses for asthenospheric melts. Asmerom interpreted this difference as a consequence of the source mineralogy at the point of initiation of melting, a spinel-bearing assemblage for the lithospheric melts and a garnet-bearing assemblage for the asthenospheric melts.

The extreme incompatible element enrichment of all the Italian volcanic rocks requires a low degree of melting, even from an already metasomatized mantle source. The occurrence of near-equilibrium to small $^{230}$Th excesses in such low-degree melts is consistent with melting occurring at relatively shallow depth, above the garnet–spinel transition zone (2·5–3·0 GPa: Green & Ringwood, 1967; Robinson & Wood, 1998).

Previous studies of the origin of the TMP and N-RMP ultrapotassic rocks have also invoked a shallow, residual (i.e. depleted) lithospheric mantle source subsequently re-fertilized by a phlogopite-rich vein network on the basis of mineralogical (Conticelli & Peccerillo, 1990; Conticelli *et al.*, 2004, and references therein), geochemical (Rogers *et al.*, 1985; Conticelli & Peccerillo, 1992) and geophysical (Peccerillo & Panza, 1999) data. This is consistent with a garnet-free source where phlogopite and amphibole do not fractionate U from Th (LaTourrette *et al.*, 1995), and a key role is played by clinopyroxene. Experimental studies (Wood *et al.*, 1999; Landwehr *et al.*, 2001) have demonstrated that partition coefficients for U and Th in clinopyroxene are strongly pressure-dependent, and that at relatively low pressure (1·5–2 GPa), little fractionation occurs.

To further constrain the depth of initiation of melting we attempted to model the U–Th disequilibria produced by the already enriched source of the TMP and N-RMP magmas in two end-member scenarios involving either a spinel- or a garnet-bearing source. Although rigorous modelling of the melting process is impossible, because of the many unknown parameters (e.g. the exact composition and mineralogy of the metasomatized source, depth and degree of melting, etc.), we believe that this calculation can be useful to constrain the depth of magma generation. To estimate the starting mante source composition we utilized the mixing calculations reported in Figs 4 and 6. The Sr and Nd isotopic composition of the TMP and N-RMP magmas requires ~3% sediment melt addition to the lithospheric mantle source. This addition would produce a metasomatized source with ~0·8 ppm Th and ~0·2 ppm U. For the model we assumed a lithospheric source with 65% olivine + 15% orthopyroxene + 13% clinopyroxene + 2% phlogopite + 5% of either spinel or garnet. For a spinel-bearing source (1·5 GPa) the bulk partition coefficient ratio $D_U/D_{Th}$ would be 1·14, derived from the following mineral/melt partition coefficients: $Kd^{l}_{Th} = 0{\cdot}000015$, $Kd^{l}_{U} = 0{\cdot}00021$, $Kd^{px}_{Th} = 0{\cdot}00077$, $Kd^{px}_{U} = 0{\cdot}0017$, $Kd^{cpx}_{Th} = 0{\cdot}027$, $Kd^{cpx}_{U} = 0{\cdot}029$ (all from McDade *et al.*, 2003: 1·5 GPa), $Kd^{phl}_{Th} = 0{\cdot}00135$, $Kd^{phl}_{U} = 0{\cdot}00113$ (LaTourrette *et al.*, 1995), and $Kd^{spn}_{Th}$ and $Kd^{spn}_{U}$ insignificant with respect to the others (e.g. Beattie, 1993). With these parameters, the ($^{230}$Th/$^{238}$U) of TMP and N-RMP rocks, along with their U and Th contents, can be generated by 1–2% batch melting.

If melting of the mantle source occurs deeper in the stability field of garnet (e.g. 3 GPa), the partition coefficients of garnet ($Kd^{gnt}_{Th} = 0{\cdot}009$, $Kd^{gnt}_{U} = 0{\cdot}028$, Salters & Longhi, 1999) and clinopyroxene at high pressure ($Kd^{cpx}_{Th} = 0{\cdot}0117$, $Kd^{cpx}_{U} = 0{\cdot}0156$ at 3 GPa, Landwehr *et al.*, 2003) drive the $D_U/D_{Th}$ value to 1·8. In this case, even without considering possible $^{230}$Th in-growth during mantle melting (e.g. dynamic melting; McKenzie, 1985), a degree of melting higher than 5% would be required to generate most of the TMP and N-RMP magmas. Such a high degree of melting, however, could not generate the extremely high Th and U contents measured even in the most primitive samples. Conversely, 1–2% melting of

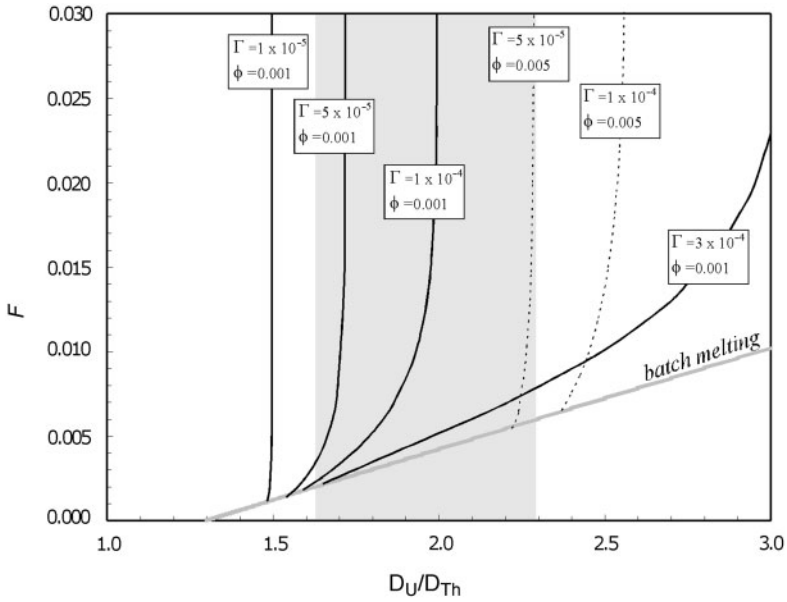


**Fig. 9.** Possible melting parameters that can produce suitable disequilibrium of the sole unaltered LuMP sample, which has $(^{230}Th/^{238}U)_i = 1{\cdot}30$. A locus of solutions using a simple batch melt is given as the thick grey curve. For dynamic melting additional parameters need to be defined. We show four illustrative loci of solutions for four melting rates (Γ) and two porosities (φ) calculated from the equations of Zou & Zindler (2000). Porosity (φ) is the fraction of total volume of rock filled by melt and represents the threshold at which the melt escapes instantaneously; further information on melting rate (Γ) and its relationships with porosity (φ), melting time and degree of melting (*F*) have been given by Zou & Zindler (2000). Clearly, a continuum of additional possible melting rates and porosities exists. Without further constraints (other U-series measurements or knowing the degree of melting), it is not possible to infer the melting rate or porosity within the underlying mantle. For the calculation $D_{Th}$ is fixed at 0·0018 as calculated for a source made up of 0·58ol + 0·22opx + 0·10cpx + 0·05gnt + 0·05phl. $D_U$ is arbitrarily varied to obtain different $D_U/D_{Th}$ ratios. The grey shaded area represents the range of $D_U/D_{Th}$ for the above-mentioned mantle source, varying the proportion of garnet from zero to 0·1 (and thus increasing $D_U/D_{Th}$). The partition coefficients used are: $Kd_{Th}^{l} = 0{\cdot}000015$, $Kd_{U}^{l} = 0{\cdot}000021$ (McDade *et al.*, 2003); $Kd_{Th}^{px} = 0{\cdot}00077$, $Kd_{U}^{px} = 0{\cdot}0017$ (McDade *et al.*, 2003); $Kd_{Th}^{cpx} = 0{\cdot}0109$, $Kd_{U}^{cpx} = 0{\cdot}01406$ (Landwehr *et al.*, 2001: at 3 GPa); $Kd_{Th}^{gnt} = 0{\cdot}009$, $Kd_{U}^{gnt} = 0{\cdot}028$ (Salters & Longhi, 1999); $Kd_{Th}^{phl} = 0{\cdot}0011$, $Kd_{U}^{phl} = 0{\cdot}0014$ (LaTourrette *et al.*, 1995).

a garnet-bearing source produces $^{230}$Th excesses as high as 8–14%, much higher than the observed values.

Although not evident in U–Th disequilibrium, a strong garnet signature is apparent in the marked HREE fractionations of the lavas (Fig. 3). Therefore, in our interpretation, the relatively fractionated REE of the studied samples are linked to the characteristics of the sediment-derived enriching agent rather than to the mantle melting process.

## $^{230}$Th excess: the Lucanian Magmatic Province

Unfortunately, this province is represented by only one reliable U-series measurement, and more data are required to confirm the basic observation and obtain a more detailed picture of the melting processes in this peculiar magmatic association. Nevertheless, the striking ~30% initial $^{230}$Th excess in the sample from the Monticchio Lake volcanic activity provides a valuable clue to understanding the differences between the LuMP magmas and those of the other Italian magmatic provinces.

Although the LuMP has been claimed to be the site of subduction-related carbonatitic magmatism (D'Orazio *et al.*, 2007), the $^{230}$Th excess of the Monticchio lakes sample (VLT 99) precludes any similarity with within-plate carbonatites, which always have extremely high U/Th values and a ubiquitous $^{238}$U excess (>40%, Williams *et al.*, 1986; Pyle *et al.*, 1991).

As outlined in the previous section, a deep garnet-bearing mantle source and possibly $^{230}$Th in-growth at low mantle porosities are required to generate large $^{230}$Th excesses (Bourdon & Sims, 2003, and references therein). The mantle source of the LuMP magmas has, therefore, to be garnet-bearing, in contrast to that of the northernmost Italian magmatic regions (i.e. TMP, N-RMP). This is also in keeping with the LuMP rocks having the highest $(La/Yb)_N$ of the entire dataset (Fig. 3 and Table 2)

The LuMP rocks have lower HFSE anomalies (Figs 3 and 6) than the rocks of the TMP and N-RMP at comparable Th and MgO contents (Fig. 2, Tables 2 and 3). Their incompatible trace element patterns (Fig. 3) are indeed intermediate between those of subduction-related and typical within-plate magmas. In addition, the LuMP rocks have the most depleted Sr and Nd isotopic signatures among the Italian alkalic volcanic rocks (Fig. 5), but have

comparable incompatible trace elements enrichments. On the whole, these geochemical and isotopic characteristics suggest the involvement of a HFSE-enriched mantle component added to a subduction-related metasomatized mantle component, similar to that of the northernmost Italian province.

The LuMP is located in an area characterized by thickened continental crust (35–45 km) but normal lithosphere thickness (90 km) (Downes *et al.*, 2002). The need for a garnet-bearing source to generate the observed $^{230}$Th excess requires melting to begin beneath the lithospheric lid. A possible mechanism for explaining both the garnet signature during recent melting and the higher HFSE contents of LuMP rocks involves the in-flow of asthenospheric mantle into the mantle wedge, following either roll-back of the Ionian subducted plate or slab detachment processes as proposed by Gvirtzman & Nur (1999) and Wortel & Spakman (2000), respectively. The position of the LuMP in the context of the Italian geodynamic setting makes the inflow of asthenospheric mantle (e.g. LVC, Hoernle *et al.*, 1995) into the mantle wedge particularly appealing. The LuMP (e.g. Monte Vulture, Monticchio lakes) is located at the northern junction between the active NW-dipping Ionian subduction zone and the old Adriatic subduction system (Fig. 1). A low-velocity zone, located at a depth of 250 km beneath the region based on seismic tomographic data (e.g. Wortel & Spakman, 2000; Piromallo & Morelli, 2003), could represent upwelling of hot mantle material and/or mantle melting. Interestingly, the same processes have been proposed to explain the clear within-plate geochemical signature, including $^{230}$Th excesses (Condomines *et al.*, 1995), of Etna (Gvirtzman & Nur, 1999), which is located in a mirror position with respect to Monte Vulture (LuMP, Fig. 1), on the southern edge of the same Ionian subduction system. Small-degree partial melts of this upwelling, garnet-bearing asthenospheric mantle could percolate the previously metasomatized lithospheric mantle beneath the area, giving rise to erupted magmatic products with trace element signatures intermediate between typical subduction-related and within-plate magmas, and significant $^{230}$Th excesses.

An attempt to model the observed $^{230}$Th excess with both batch and dynamic melting models is illustrated in Fig. 9. In batch melting models, the amount of disequilibrium produced depends only on the partition coefficients of U and Th and the degree of melting. Figure 9 shows that for a wide range of $D_U/D_{Th}$ values, the degree of melting required to generate the observed disequilibria is extremely low (<1%). The dynamic melting model (McKenzie, 1985) is able produce a suitably high $^{230}$Th excess at higher degrees of melting, as it takes into account the duration of the melting process and thus the in-growth of $^{230}$Th in the residual solid. This model depends on two key additional parameters: the melting rate ($\Gamma$) and mantle porosity ($\varphi$). Given these further unknowns, it is impossible to constrain properly the melting regime with only U–Th disequilibria, and Fig. 9 shows a range of plausible conditions. For the most probable range of U and Th partition coefficients, a component of dynamic melting is needed if the degree of melting is >1%. Unfortunately, the degree of melting is difficult to estimate and so it is hard to definitively invoke a component of in-growth and thus infer upwelling.

## CONCLUDING REMARKS

Neogene potassic (shoshonitic) and ultrapotassic magmas from the Italian region are generated from an originally depleted lithospheric mantle source strongly metasomatized by subduction-related fluids or melts. The geochemical and isotopic characteristics of the studied rocks indicate a common metasomatic event across the whole Italian area. Sedimentary materials with variable compositions have been subducted along with the Adriatic slab and transported into the overlying mantle as partial melts or supercritical liquids. U–Th data for the TMP and N-RMP rocks are consistent with subsequent melting episodes not directly related to subduction processes, but occurring in response to post-collisional lithospheric stretching related to the opening of the Tyrrhenian back-arc basins. The lack of U–Th disequilibrium in these rocks indicates a relatively shallow origin in a garnet-free metasomatized lithospheric mantle source (<85 km). The garnet signature in the trace element patterns of these rocks does not represent a melting signature, but it is inherited from the sediment-derived melt that metasomatized the mantle source at >400 ka.

The occurrence of strong $^{238}$U excesses in the rocks from the ND requires U addition, shortly before melting. This component must be sufficiently enriched in U to affect the ($^{230}$Th/$^{238}$U) of the already U- and Th-enriched mantle beneath the area. We envisage that this U-rich component is related to the still-active oceanic Ionian subduction zone. At the anomalous depth (>350 km) reached by the Ionian slab beneath the Neapolitan area, the clay–carbonate-rich sedimentary assemblage subducted on top of the slab releases supercritical liquids highly enriched in U over Th. We suggest that these supercritical liquids are able to transport a higher amount of U (and other mobile trace elements) than the simple aqueous fluids generated in normal sub-arc conditions, and thus to produce the observed $^{238}$U excesses.

The rocks from the LuMP have smaller HFSE negative anomalies than those from all the other provinces and the sole unaltered sample displays ~30% $^{230}$Th excess. These features require the involvement of a HFSE-enriched component and constrain melting at pressures within the stability field of garnet (>85 km). The inflow of asthenospheric material in response to slab detachment

and roll-back of the Ionian plate (Wortel & Spakman, 2000) is a likely candidate to explain the geochemical and isotopic characteristics of the LuMP magmas. The high $^{230}$Th excess hints at the need for dynamic melting processes at low porosity and melting rate, but further U-series measurements would be required to make this a firm constraint.

## ACKNOWLEDGEMENTS

We would like to thank Elena Boari, Giulia Perini, Raffaello Cioni, Vincenzo Morra, Leone Melluso, Lorella Francalanci and Massimo D'Antonio for providing samples and unpublished analytical results, Lucia Civetta and Massimo D'Antonio for allowing access to Mass Spectrometer Facilities of Naples, and Maurizio Ulivi, Chiara M. Petrone, Giulia Perini and Lorella Francalanci for helping with Sr and Nd isotopic analyses in Florence, and for critical reading of an early version of the manuscript. Dirk Hoffmann and Chris Coath are also acknowledged for the invaluable support in U–Th measurements and data processing and correction, and Julie Prytulak for a critical reading of the manuscript. The manuscript was greatly improved by constructive reviews of Georg Zellmer, John Wolff and an anonymous reviewer, and by the comments of the editor Wendy Bohrson. This research was supported by FIRB 2001 grant RBAU01FX8_M_003 and PRIN 2004 grant 2004040502_001 grants issued by 'MIUR' to S.C. and PRIN 2007 grant 2007NS22NZ-005 issued to S.T.

## REFERENCES

Altherr, R., Meyer, H.-P., Holl, A., Volker, F., Alibert, C., McCulloch, M. T. & Majer, V. (2004). Geochemical and Sr–Nd–Pb isotopic characteristics of late Cenozoic leucite lamproites from the East European Alpine belt (Macedonia and Yugoslavia). *Contributions to Mineralogy and Petrology* **147**, 58–73.

Anderson, H. & Jackson, J. A. (1987*a*). Active tectonics of the Adriatic region. *Geophysical Journal of the Royal Astronomical Society* **91**, 937–983.

Anderson, H. & Jackson, J. A. (1987*b*). Deep seismicity of the Tyrrhenian Sea. *Geophysical Journal of the Royal Astronomical Society* **91**, 613–637.

Asmerom, Y. (1999). Th–U fractionation and mantle structure. *Earth and Planetary Science Letters* **166**, 163–175.

Asmerom, Y. & Edwards, R. L. (1995). U-series isotope evidence for the origin of continental basalts. *Earth and Planetary Science Letters* **134**, 1–7.

Asmerom, Y., Cheng, H., Thomas, R., Hirschmann, M. & Edwards, R. L. (2000). Melting of the Earth's lithospheric mantle inferred from protactinium–thorium–uranium isotopic data. *Nature* **406**, 293–296.

Avanzinelli, R., Boari, E., Conticelli, S., Francalanci, L., Guarnieri, L., Perini, G., Petrone, C. M., Tommasini, S. & Ulivi, M. (2005). High precision Sr, Nd, and Pb isotopic analyses using new generation thermal ionisation mass spectrometer: aims and perspective for isotope geology applications. *Periodico di Mineralogia* **74**, 147–166.

Ball, L., Sims, K, Schwieters, J. B. & Tuttas, D. (2004). Thorium isotopic composition of synthetic standards measured by the Finnigan NEPTUNE and Finnigan TRITON. *Geochimica et Cosmochimica Acta* **68**, (11S): 542.

Beattie, P. (1993). The generation of uranium series disequilibria by partial melting of spinel peridotite; constraints from partitioning studies. *Earth and Planetary Science Letters* **117**, 379–391.

Beccaluva, L., Di Girolamo, P. & Serri, G. (1991). Petrogenesis and tectonic setting of the Roman Volcanic Province, Italy. *Lithos* **26**, 191–221.

Bell, K., Castorina, F., Lavecchia, G., Rosatelli, G. & Stoppa, F. (2004). Is there a mantle plume below Italy? *EOS Transactions, American Geophysical Union* **85**, 541–547.

Berlo, K., Turner, S., Blundy, J. & Hawkesworth, C. J. (2004). The extent of U-series disequilibria produced during partial melting of the lower crust with implications for the formation of the Mount St. Helens dacites. *Contributions to Mineralogy and Petrology* **148**, 122–130.

Bigazzi, G., Bonadonna, F. P., Ghezzo, C., Giuliani, O., Radicati di Bronzolo, F. & Rita, F. (1981). Geochronological study of the Monte Amiata lavas (Central Italy). *Bulletin of Volcanology* **44**, 455–465.

Bindi, L., Cellai, D., Melluso, L., Conticelli, S., Morra, V. & Menchetti, S. (1999). Crystal chemistry of clinopyroxene from alkaline undersaturated rocks of the Monte Vulture Volcano, Italy. *Lithos* **46**, 259–274.

Black, S., Macdonald, R., DeVivo, B., Kilburn, C. R. J. & Rolandi, G. (1998). U-series disequilibria in young A.D. 1944 Vesuvius rocks: Preliminary implications for magma residence times and volatile addition. *Journal of Volcanology and Geothermal Research* **82**, 97–111.

Boari, E. & Conticelli, S. (2008). Mineralogy and petrology of Mg-rich calc-alkalic, potassic, and ultrapotassic associated rocks: the Middle Latin Valley monogenetic volcanoes, Roman Magmatic Province, Southern Italy. *Canadian Mineralogist* (in press).

Bohrson, W. A. & Spera, F. J. (2001). Energy-constrained open-system magmatic processes II: application of energy-constrained assimilation–fractional crystallization (EC-AFC) model to magmatic systems. *Journal of Petrology* **42**, 1019–1041.

Bohrson, W. A., Spera, F. J., Fowler, S. J., Belkin, H. E., DeVivo, B. & Rolandi, G. (2006). Petrogenesis of the Campanian Ignimbrite: implications for crystal–melt separation and open-system processes from major and trace elements and Th isotope data. In: De Vivo, B. (ed.) *Volcanism in the Campania Plain, Vesuvius, Campi Flegrei and Ignimbrites. Developments in Volcanology* **9**, 249–288.

Bourdon, B. & Sims, K. W. W. (2003). U-series constraints on intraplate basaltic magmatisms. In: Bourdon, B., Henderson, G. M., Lundstrom, C. C. & Turner, S. P. (eds) *Uranium Series Geochemistry. Mineralogical Society of America, Reviews in Mineralogy and Geochemistry* **52**, 215–254.

Brocchini, D., La Volpe, L., Laurenzi, M. A. & Principe, C. (1994). Storia evolutiva del Monte Vulture. *Plinius* **12**, 22–25.

Capaldi, G., Cortini, M. & Pece, R. (1982). Th isotopes at Vesuvius: evidence for open system behaviour of magma-forming processes. *Journal of Volcanology and Geothermal Research* **14**, 247–260.

Carminati, E., Wortel, M. J. R., Spakman, W. & Sabadini, R. (1998). A new model for the opening of the western–central Mediterranean basins: geological and geophysical constraints for a major role of slab detachment. *Earth and Planetary Science Letters* **160**, 651–665.

Chelazzi, L., Bindi, L., Olmi, F., Peccerillo, A., Menchetti, S. & Conticelli, S. (2006). A lamproitic component in the high-K

calc-alkaline volcanic rocks of the Capraia Island, Tuscan Magmatic Province: evidence from clinopyroxene crystal chemical data. *Periodico di Mineralogia* **75**, 75–94.

Class, C., Miller, D. M., Goldstein, S. L. & Langmuir, C. H. (2000). Distinguishing melt and fluid subduction components in Umnak volcanics, Aleutinian arc. *Geochemistry, Geophysics, Geosystems* **1**, paper number 1999GC000010.

Cohen, A. S., O'Nions, R. K. & Kurz, M. D. (1996). Chemical and isotopic variations in Mauna Loa tholeiites. *Earth and Planetary Science Letters* **143**, 111–124.

Condomines, M. & Sigmarsson, O. (1993). Why are so many magmas close to $^{238}U$–$^{230}Th$ radioactive equilibrium? *Geochimica et Cosmochimica Acta* **57**, 4491–4497.

Condomines, M., Hemond, C. & Allègre, C. J. (1988). U–Th–Ra radioactive disequilibria and magmatic processes. *Earth and Planetary Science Letters* **90**, 243–262.

Condomines, M., Tanguy, J.-C. & Michaud, V. (1995). Magma dynamics at Mt. Etna: constraints from U–Th–Ra–Pb radioactive disequilibria and Sr isotopes in historical lavas. *Earth and Planetary Science Letters* **123**, 25–41.

Conticelli, S. (1998). Effects of crustal contamination on ultrapotassic magmas with lamproitic affinity: mineralogical, geochemical and isotope data from the Torre Alfina lavas and xenoliths, Central Italy. *Chemical Geology* **149**, 51–81, doi:10.1016/S0009-2541(98)00038-2.

Conticelli, S. & Peccerillo, A. (1990). Petrological significance of high-pressure ultramafic xenoliths from ultrapotassic rocks of Central Italy. *Lithos* **24**, 305–322.

Conticelli, S. & Peccerillo, A. (1992). Petrology and geochemistry of potassic and ultrapotassic volcanism in central Italy: petrogenesis and inferences on the evolution of the mantle sources. *Lithos* **28**, 221–240.

Conticelli, S., Francalanci, L. & Santo, A. P. (1991). Petrology of the final stage Latera lavas: mineralogical, geochemical and Sr-isotopic data and their bearing on the genesis of some potassic magmas in Central Italy. *Journal of Volcanology and Geothermal Research* **46**, 187–212.

Conticelli, S., Manetti, P. & Menichetti, S. (1992). Petrology, chemistry, mineralogy and Sr-isotopic features of Pliocenic orendites from South Tuscany: implications on their genesis and evolutions. *European Journal of Mineralogy* **4**, 1359–1375.

Conticelli, S., Francalanci, L., Manetti, P., Cioni, R. & Sbrana, A. (1997). Petrology and geochemistry of the ultrapotassic rocks from the Sabatini Volcanic District, Central Italy: the role of evolutionary processes in the genesis of variably enriched alkaline magmas. *Journal of Volcanology and Geothermal Research* **75**, 107–136, doi:10.1016/S0377-0273(96)00062-5.

Conticelli, S., D'Antonio, M., Pinarelli, L. & Civetta, L. (2002). Source contamination and mantle heterogeneity in the genesis of Italian potassic and ultrapotassic volcanic rocks: Sr–Nd–Pb isotope data from Roman Province and Southern Tuscany. *Mineralogy and Petrology* **74**, 189–222, doi:10.1007/s007100200004.

Conticelli, S., Melluso, L., Perini, G., Avanzinelli, R. & Boari, E. (2004). Petrologic, geochemical, and isotopic characteristics of potassic and ultrapotassic magmatism in Central–Southern Italy: inferences on its genesis and on the nature of mantle sources. *Periodico di Mineralogia* **73**(1), 153–164.

Conticelli, S., Carlson, R. W., Widom, E. & Serri, G. (2007). Chemical and isotopic composition (Os, Pb, Nd, and Sr) of Neogene to Quaternary calc-alkalic, shoshonitic, and ultrapotassic mafic rocks from the Italian peninsula: Inferences on the nature of their mantle sources. In: Beccaluva, L., Bianchini, G. & Wilson, M. (eds) *Cenozoic Volcanism in the Mediterranean Area. Geological Society of America, Special Papers* **418**, 171–202, doi:10.1130/2007.2418(09).

Cortini, M., Ayuso, R. A., De Vivo, B., Holden, P. & Somma, R. (2004). Isotopic composition of Pb and Th in interplinian volcanics from Somma–Vesuvius volcano, Italy. *Mineralogy and Petrology* **80**, 83–96.

Della Vedova, B., Pellis, G., Foucher, J. P. & Rehault, J. P. (1984). Geothermal structure of the Tyrrhenian Sea. *Marine Geology* **55**, 271–289.

Del Moro, A., Fulignati, P., Marianelli, P. & Sbrana, A. (2001). Magma contamination by direct wall-rock interaction: constraints from xenoliths from the walls of a carbonate-hosted magma chamber (Vesuvius 1944 eruption). *Journal of Volcanology and Geothermal Research* **112**, 15–24.

Dewey, J. F., Helman, M. L. & Turco, E. (1989). Kinematics of the Western Mediterranean. In: Coward, M. P., Dietrich, D. & Park, R. G. (eds) *Alpine Tectonics. Geological Society, London, Special Publications* **45**, 265–283.

Di Girolamo, P., Melluso, L., Morra, V. & Secchi, F. A. G. (1995). Evidence of interaction between mafic and intermediate magmas in the youngest activity phase at Ischia Island. *Periodico di Mineralogia* **64**, 393–411.

D'Orazio, M., Innocenti, F., Tonarini, S. & Doglioni, C. (2007). Carbonatites in a subduction system: the Pleistocene alvikites from Mt. Vulture (Southern Italy. *Lithos,* doi:10.1016/j.lithos.2007.05.004.

Downes, H. (2001). Formation and modification of the shallow sub-continental lithospheric mantle: a review of geochemical evidence from ultramafic xenolith suites and tectonically emplaced ultramafic massifs of Western and Central Europe. *Journal of Petrology* **42**, 233–250.

Downes, H., Kostoula, T., Jones, A. P., Beard, A. D., Thirlwall, M. F. & Bodinier, J.-L. (2002). Geochemistry and Sr–Nd isotopic compositions of mantle xenoliths from the Monte Vulture carbonatite–melilitite volcano, central southern Italy. *Contributions to Mineralogy and Petrology* **144**, 78–92.

Duggen, S., Hoernle, K., van den Bogaard, P. & Harris, C. (2004). Magmatic evolution of the Alboran region: The role of subduction in forming the Western Mediterranean and causing the Messinian salinity chrisis. *Earth and Planetary Science Letters* **218**, 91–108.

Elliott, T. R., Plank, T., Zindler, A., White, W. & Bourdon, B. (1997). Element transport from slab to volcanic front at the Mariana arc. *Journal of Geophysical Research* **102**, 14991–15019.

Faccenna, C., Funiciello, F., Giardini, D. & Lucente, P. (2001). Episodic back-arc extension during restricted mantle convection in the Central Mediterranean. *Earth and Planetary Science Letters* **187**, 105–116.

Ferrari, L., Conticelli, S., Burlamacchi, L. & Manetti, P. (1996). Volcanological evolution of the Monte Amiata Volcanic Center, Southern Tuscany, Central Italy: new geological and petrochemical data. *Acta Vulcanologica* **8**, 41–56.

Foley, S. F. (1992). Vein-plus-wall-rock melting mechanisms in the lithosphere and the origin of potassic alkaline magmas. *Lithos* **28**, 435–453.

Fornaseri, M. (1985). Geochronology of volcanic rocks from Latium (Italy). *Rendiconti della Società Italiana di Mineralogia e Petrologia* **40**, 73–105.

Francalanci, L., Avanzinelli, R., Tommasini, S. & Heumann A. (2007). A west–east geochemical and isotopic traverse along the subaerial volcanism of the Aeolian arc, Southern Tyrrhenian Sea: inferences on mantle source processes. In: Beccaluva, L., Bianchini, G. & Wilson, M. (eds) *Cenozoic Volcanism in the Mediterranean Area. Geological Society of America, Special Papers* **418**, 235–263, doi:10.1130/2007.2418(12).

Franzini, M., Leoni, I. & Saitta, M. (1972). A simple method to evaluate the matrix effects in X-ray fluorescence analyses. *X-ray Spectrometry* **1**, 151–154.

Gasperini, D., Blichert-Toft, J., Bosh, D., Del Moro, A., Macera, P. & Albarède, F. (2002). Upwelling of deep mantle material through a plate window: evidence from geochemistry of Italian basaltic volcanics. *Journal of Geophysical Research* **107**, 2367–2386.

Gill, J. B. & Condomines, M. (1992). Short-lived radioactivity and magma genesis. *Science* **257**, 1368–1376.

Gill, J. B. & Williams, R. W. (1990). Th isotope and U-series studies of subduction-related volcanic rocks. *Geochimica et Cosmochimica Acta* **54**, 1427–1442.

Green, D. H. & Ringwood, A. E. (1967). The stability field of aluminous pyroxene peridotite and garnet peridotite and their relevance in upper mantle structure. *Earth and Planetary Science Letters* **3**, 151–120.

Gvirtzman, Z. & Nur, A. (1999). The formation of Mount Etna as the consequence of slab rollback. *Nature* **401**, 782–785.

Hawkesworth, C. J. & Vollmer, R. (1979). Crustal contamination versus enriched mantle: $^{143}Nd/^{144}Nd$ and $^{87}Sr/^{86}Sr$ evidence from the Italian volcanics. *Contributions to Mineralogy and Petrology* **69**, 151–165.

Hawkesworth, C. J., Gallagher, K., Hergt, J. M. & McDermott, F. (1993). Mantle and slab contributions in arc magmas. *Annual Review of Earth and Planetary Sciences* **21**, 175–204.

Hawkesworth, C. J., Turner, S. P., Peate, D. W., McDermott, F. & van Calsteren, P. (1997). U–Th isotopes in arc magmas: implications for element transfer from the subducted crust. *Science* **276**, 551–555.

Hermann, J., Spandler, C., Hack, A. & Korsakov, A. V. (2006). Aqueous fluids and hydrous melts in high-pressure and ultra-high pressure rocks: Implications for element transfer in subduction zones. *Lithos* **92**, 399–417.

Hoernle, K., Zhang, Y.-S. & Graham, D. (1995). Seismic and geochemical evidence for large-scale mantle upwelling beneath the eastern Atlantic and western and central Europe. *Nature* **374**, 34–39.

Hoffmann, D. L., Richards, D. A., Elliott, T. R., Smart, P. L. & Hawkesworth, C. J. (2005). Studies on the linearity of a secondary electron multiplier (SEM) using MC-ICPMS—alternative approach for nonlinearity characterisation. *International Journal of Mass Spectrometry* **244**, 97–108.

Hoffmann, D. L., Prytulak, J., Richards, D. A., Elliott, T., Coath, C. D., Smart, P. L. & Scholz, D. (2007). Procedures for accurate U and Th isotope measurements by high precision MC-ICPMS. *International Journal of Mass Spectrometry* **264**, 97–109.

Hoogewerff, J. A., VanBergen, M. J., Vroon, P. Z., Hertogen, J., Wordel, R., Sneyers, A., Nasution, A., Varekamp, J. C., Moens, H. L. E. & Mouchel, D. (1997). U-series, Sr–Nd–Pb isotope and trace element systematics across an active island arc–continent collision zone: implications for element transfer at the slab–wedge interface. *Geochimica et Cosmochimica Acta* **61**, 1057–1072.

Ivanovich, M. & Harmon, R. S. (1992). *Uranium Series Disequilibrium: Application to Earth, Marine, and Environmental Science*. Oxford: Oxford University Press.

Johnson, M. C. & Plank, T. (1999). Dehydration and melting experiments constrain the fate of subducted sediments. *Geochemistry, Geophysics, Geosystem* **1**, paper number 1999GC000014.

Kerrick, D. M. & Connolly, J. A. D. (2001). Metamorphic devolatilization of subducted marine sediments and the transport of volatiles into the Earth's mantle. *Nature* **411**, 293–296.

Kessel, R., Schmidt, M. W., Ulmer, P. & Pettke, T. (2005). Trace element signature of subduction-zone fluids, melts and supercritical liquids at 120–180 km depth. *Nature* **437**, 724–727.

Krom, M. D., Michard, A., Cliff, R. A. & Strohle, K. (1999). Sources of sediment to the Ionian Sea and western Levantine basin of the Eastern Mediterranean during S-1 sapropel times. *Marine Geology* **160**, 45–61.

Landwehr, D., Blundy, J., Chamorro-Perez, E., Hill, E. & Wood, B. (2001). U-series disequilibria generated by partial melting of spinel lherzolite. *Earth and Planetary Science Letters* **188**, 329–348.

LaTourrette, T. Z., Hervig, R. L. & Holloway, J. R. (1995). Trace element partitioning between amphibole phlogopite and basanite melt. *Earth and Planetary Science Letters* **135**, 13–30.

Marra, F., Taddeucci, J., Freda, C., Marzocchi, W. & Scarlato, P. (2004). Recurrence of volcanic activity along the Roman Comagmatic Province (Tyrrhenian margin of Italy) and its tectonic significance. *Tectonics* **23**, TC4013, doi:10.1029/2003TC001600.

McDade, P., Blundy, J. D. & Wood, B.J. (2003). Trace element partitioning on the Tinaquillo Lherzolite solidus at 1·5 GPa. *Physics of the Earth and Planetary Interiors* **139**, 129–147.

McDermott, F. & Hawkesworth, C. J. (1991). Thorium, lead and strontium isotopes in young island arc volcanics and oceanic sediments. *Earth and Planetary Science Letters* **104**, 1–15.

McKenzie, D. P. (1985). $^{230}Th–^{236}U$ disequilibrium and the melting processes beneath ridge axes. *Earth and Planetary Science Letters* **72**, 149–167.

Mele, G., Rivelli, A., Seber, D. & Baranzangi, M. (1996). Lateral variations of Pn propagation in Italy: evidence for a high attenuation zone beneath the Apennines. *Geophysical Research Letters* **23**, 709–712.

Melluso, L., Morra, V., Perrotta, A., Scarpati, C. & Addabbo, M. (1995). The eruption of the Breccia Museo (Campi Flegrei, Italy): fractional crystallisation processes in a shallow, zoned magma chamber and implication for the eruptive dynamics. *Journal of Volcanology and Geothermal Research* **68**, 325–339.

Melluso, L., Conticelli, S., D'Antonio, M., Mirco, N. & Saccani, E. (2003). Petrology and mineralogy of wollastonite- and melilite-bearing paralavas from Central Apennines, Italy. *American Mineralogist* **88**, 1287–1299.

Molina, J. F. & Poli, S. (2000). Carbonate stability and fuid composition in subducted oceanic crust: an experimental study on $H_2O$–$CO_2$-bearing basalts. *Earth and Planetary Science Letters* **176**, 295–310.

Mongelli, G. & Dinelli, E. (2001). The geochemistry of shales from the 'Frido Unit', Liguride Complex, Lucanian Apennines, Italy: Implications for provenance and tectonic setting. *Ofioliti* **26**, 457–466.

Newman, S., Macdougall, J. D. & Finkel, R. C. (1984). $^{230}Th–^{238}U$ disequilibrium in arc lavas: evidence from the Aleutians and the Marianas. *Nature* **308**, 226–270.

Nichols, G. T., Wyllie, P. J. & Stern, J. R. (1994). Subduction zone melting of pelagic sediments constrained by melting experiment. *Nature* **371**, 785–788.

Nicholson, H., Condomines, M., Fitton, J. G., Fallick, A. E., Grönvold, K. & Rogers, G. (1991). Geochemical and isotopic evidence for crustal assimilation beneath Krafla, Iceland. *Journal of Petrology* **32**, 1005–1020.

Peccerillo, A. (1985). Roman Comagmatic Province (Central Italy): Evidence for subduction related magma genesis. *Geology* **13**, 103–106.

Peccerillo, A. & Panza, G. F. (1999). Upper mantle domains beneath central–southern Italy: petrological, geochemical and geophysical constraints. *Pure and Applied Geophysics* **156**, 421–443.

Perini, G., Tepley, F. J., III, Davidson, J. P. & Conticelli, S. (2003). The origin of K-feldspar megacrysts hosted in alkaline potassic rocks: track for low pressure processes in primitive magmas. *Lithos* **66**, 223–240, doi:10.1016/S0024-4937(02)00221-9.

Perini, G., Francalanci, L., Davidson, J. P. & Conticelli, S. (2004). Evolution and genesis of magmas from Vico Volcano, Central Italy: multiple differentiation pathways and variable parental magmas. *Journal of Petrology* **45**, 139–182, doi:10.1093/petrology/egg084.

Pietruszka, A. J., Carlson, R. W. & Hauri, E. H. (2002). Precise and accurate measurement of $^{226}Ra$–$^{230}Th$–$^{238}U$ disequilibria in volcanic rocks using plasma ionization multicollector mass spectrometry. *Chemical Geology* **188**, 171–191.

Piromallo, C. & Morelli, A. (2003). P-wave tomography of the mantle under the Alpine–Mediterranean area. *Journal of Geophysical Research* **108**(B2), 2065, doi:10.1029/2002JB001757.

Plank, T. (2005). Constraints from thorium/lanthanum on sediment recycling at subduction zones and the evolution of the continents. *Journal of Petrology* **46**, 921–944.

Plank, T. & Langmuir, C. H. (1998). The chemical composition of subducting sediment and its consequences for the crust and mantle. *Chemical Geology* **145**, 325–394.

Poli, S., Chiesa, S., Gillot, P. Y., Gregnanin, A. & Guichard, F. (1987). Chemistry versus time in the volcanic complex of Ischia (Gulf of Naples, Italy): evidence of successive magmatic cycle. *Contributions to Mineralogy and Petrology* **95**, 322–335.

Porcelli, D. & Swarzenski, P. W. (2003). The behaviour of U- and Th-series nuclides in groundwater. In: Bourdon, B., Henderson, G. M., Lundstrom, C. C. & Turner, S. P. (eds) *Uranium Series Geochemistry. Mineralogical Society of America, Reviews in Mineralogy and Geochemistry* **52**, 317–361.

Prelević, D., Foley, S. F., Cvetković, V. & Romer, R. L. (2004). Origin of minette by mixing of lamproite and dacite magmas in Veliki Majdan, Serbia. *Journal of Petrology* **45**, 759–792.

Principe, C., Tanguy, J. C., Arrighi, S., Palotti, A., Le Goff, M. & Zoppi, U. (2004). Chronology of Vesuvius activity from A.D. 79 to 1631 based on archaeomagnetism of lavas of historical sources. *Bulletin of Volcanology* **66**, 703–724.

Pyle, D. M., Dawson, J. B. & Ivanovich, M. (1991). Short-lived decay series disequilibria in the natrocarbonatite lavas of Oldoinyo Lengai, Tanzania: constraints on the timing of magma genesis. *Earth and Planetary Science Letters* **105**, 378–396.

Reid, M. R. (1995). Processes of mantle enrichment and magmatic differentiation in the Eastern Snake River Plain: Th isotope evidence. *Earth and Planetary Science Letters* **131**, 239–254.

Reid, M. R. & Ramos, F. C. (1996). Chemical dynamics of enriched mantle in the South-Western United States: Thorium isotope evidence. *Earth and Planetary Science Letters* **138**, 67–81.

Richter, S., Goldberg, S. A., Mason, P. B., Traina, A. J. & Schwieters, J. B. (2001). Linearity test for secondary electron multipliers used in isotope ratio mass spectrometry. *International Journal of Mass Spectrometry* **206**, 105–127.

Robinson, J. A. C. & Wood, B. J. (1998). The depth of spinel to garnet transition at the peridotite solidus. *Earth and Planetary Science Letters* **164**, 277–284.

Rogers, N. W., Hawkesworth, C. J., Parker, R. J. & Marsh, J. S. (1985). The geochemistry of potassic lavas from Vulsini, Central Italy, and implications for mantle enrichment processes beneath the Roman region. *Contributions to Mineralogy and Petrology* **90**, 244–257.

Rosholt, J. N. & Noble, D. C. (1969). Loss of uranium from crystallized silicic volcanic rocks. *Earth and Planetary Science Letters* **6**, 268–270.

Rosholt, J. N., Zartman, R. E. & Nkomo, I. T. (1973). Lead isotope systematics and uranium depletion in Granite Mountains, Wyoming. *Geological Society of America Bulletin* **84**, 989–1002.

Rüpke, L. H., Phipps Morgan, J., Hort, M. & Connolly, J. A. D. (2004). Serpentine and the subduction zone water cycle. *Earth and Planetary Science Letters* **223**, 17–34.

Salters, V. J. M. & Longhi, J. (1999). Trace element partitioning during the initial stage of melting beneath mid ocean ridges. *Earth and Planetary Science Letters* **166**, 15–30.

Savelli, C. (2000). Subduction-related episodes of K-alkaline magmatism (15–0 Ma) and geodynamic implications in the north Tyrrhenian–central Italy region: a review. *Journal of Geodynamics* **30**, 575–591.

Schiano, P., Clocchiatti, R., Ottolini, L. & Sbrana, A. (2004). The relationship between potassic, calc-alkaline and Na-alkaline in South Italy volcanoes: a melt inclusion approach. *Earth and Planetary Science Letters* **220**, 121–137.

Schmidt, M. W., Vielzeuf, D. & Auzanneau, E. (2004). Melting and dissolution of subducting crust at high pressures: the key role of white mica. *Earth and Planetary Science Letters* **228**, 65–84.

Selvaggi, G. & Amato, A. (1992). Subcrustal earthquakes in the Northern Apennines (Italy): evidence for a still active subduction? *Geophysical Research Letters* **21**, 2127–2130.

Selvaggi, G. & Chiarabba, C. (1995). Seismicity and P-wave velocity image of the Southern Tyrrhenian subduction zone. *US Geophysical Journal International* **122**, 818–826.

Shapiro, L. & Brannock, W. W. (1962). Rapid analyses of silicate, carbonate and phosphate rocks. *US Geological Survey Bulletin* **1144**, 1–55.

Spera, F. J. & Bohrson, W. A. (2001). Energy-constrained open-system magmatic processes I: general model and energy-constrained assimilation–fractional crystallisation (EC-AFC) formulation. *Journal of Petrology* **42**, 999–1018.

Stoppa, F. & Lavecchia, G. (1992). Late Pleistocene ultra-alkaline magmatic activity in the Umbria–Latium region: an overview. *Journal of Volcanology and Geothermal Research* **52**, 277–293.

Sun, S-s. & McDonough, W. F. (1989). Chemical and isotopic systematics of ocean basalts: implication for mantle composition and processes. In: Saunders, A. D. & Norry, M. J. (eds) *Magmatism in the Ocean Basins. Geological Society, London, Special Publications* **42**, 313–345.

Tommasini, S., Heumann, A., Avanzinelli, R. & Francalanci, L. (2007). The fate of high angle dipping slabs in the subduction factory: an integrated trace element and radiogenic isotope (U, Th, Sr, Nd, Pb) study of Stromboli Volcano, Aeolian Arc, Italy. *Journal of Petrology* **48**, 2407–2430.

Treves, B. (1984). Orogenic belts as accretionary prisms: the example of the Northern Apennines. *Ofioliti* **9**, 577–618.

Turner, S. P., Hawkesworth, C. J., van Calsteren, P., Heath, E., Macdonald, R. & Black, S. (1996). U-series isotopes and destructive plate margin magma genesis in the Lesser Antilles. *Earth and Planetary Science Letters* **142**, 191–207.

Turner, S. P., Bourdon, B. & Gill, J. (2003). Insights into magma genesis at convergent margins from U-series isotopes. In: Bourdon, B., Henderson, G. M., Lundstrom, C. C. & Turner, S. P. (eds). *Uranium Series Geochemistry. Mineralogical Society of America, Reviews in Mineralogy and Geochemistry* **52**, 255–315.

Venturelli, G., Capedri, S., Di Battistini, G., Crawford, A. J., Kogarko, L. N. & Celestini, S. (1984*a*). The ultrapotassic rocks fron souteastern Spain. *Lithos* **17**, 37–54.

Venturelli, G., Thorpe, R. S., Dal Piaz, G. V., Del Moro, A. & Potts, P. J. (1984*b*). Petrogenesis of calc-alkaline, shoshonitic and associated ultrapotassic Oligocene volcanic rocks from Northwestern Alps, Italy. *Contributions to Mineralogy and Petrology* **86**, 209–220.

Villemant, B. & Flehoc, C. (1989). U–Th fractionation by fluids in K-rich magma genesis: the Vico volcano, Central Italy. *Earth and Planetary Science Letters* **91**, 312–326.

Vollmer, R. (1976). Rb–Sr and U–Th–Pb systematics of alkaline rocks: the alkaline rocks from Italy. *Geochimica et Cosmochimic Acta* **40**, 283–295.

Vollmer, R. & Hawkesworth, C. J. (1980). Lead isotopic composition of the potassic rocks from Roccamonfina (South Italy). *Earth and Planetary Science Letters* **47**, 91–101.

Voltaggio, M., Andretta, D. & Taddeucci, A. (1994). $^{230}$Th–$^{238}$U data in conflict with $^{40}$Ar/$^{39}$Ar leucite ages for Quaternary volcanic rocks of the Alban Hills, Italy. *European Journal of Mineralogy* **6**, 209–216.

Voltaggio, M., Branca, M., Teduesco, D., Tuccimei, P. & Di Pietro, L. (2004). $^{226}$Ra-excess during the 1631–1944 activity period of Vesuvius (Italy): a model of alpha-recoil enrichment in a metasomatized mantle and implications on the current state of the magmatic system. *Geochimica et Cosmochimica Acta* **68**, 167–181.

Vroon, P. Z., Vanbergen, M. J., White, W. M. & Varekamp, J. C. (1993). Sr–Nd–Pb isotope systematic of Banda arc Indonesia; Combined subduction and assimilation material. *Journal of Geophysical Research* **98**, 22349–22366.

Wagner, C. & Velde, D. (1986). The mineralogy of K-richterite bearing lamproite. *American Mineralogist* **71**, 17–37.

Washington, H. S. (1906). The Roman Comagmatic Region. *Carnegie Institution of Washington Yearbook* **36**, 1–220.

Weldeab, S., Emeis, K. C., Hemleben, C. & Siebel, W. (2002). Provenance of lithogenic surface sediments and pathways of riverine suspended matter in the Eastern Mediterranean Sea: evidence from $^{143}$Nd/$^{144}$Nd and $^{87}$Sr/$^{86}$Sr ratios. *Chemical Geology* **186**, 139–149.

Wendlandt, R. F. & Eggler, D. H. (1980*a*). The origin of potassic magmas: 1. Melting relations in the systems $KAlSiO_4$–$Mg_2SiO_4$–$SiO_2$ and $KAlSiO_4$–MgO–$SiO_2$–$CO_2$ to 30 kb. *American Journal of Science* **280**, 385–420.

Wendlandt, R. F. & Eggler, D. H. (1980*b*). The origin of potassic magmas: 2. Stability of phlogopite in natural spinel lherzolite and in the system $KAlSiO_4$–MgO–$SiO_2$–$H_2O$–$CO_2$ at high pressure and high temperature. *American Journal of Science* **280**, 421–458.

Whitford, D. J., Nichols, I. A. & Taylor, S. R. (1979). Spatial variations in the geochemistry of Quaternary lavas across the Sunda Arc in Java and Bali. *Contributions to Mineralogy and Petrology* **70**, 341–356.

Williams, R. W., Gill, J. B. & Bruland, K. W. (1986). Ra–Th disequilibria systematics: timescale of carbonatite magma formation at Oldoinyo Lengai volcano, Tanzania. *Geochimica et Cosmochimica Acta* **50**, 1249–1259.

Wood, B. J., Blundy, J. D. & Robinson, A. C. (1999). The role of clinopyroxene in generating U-series disequilibrium during mantle melting. *Geochimica et Cosmochimica Acta* **63**, 1613–1620.

Workman, R. H. & Hart, S. R. (2005). Major and trace element composition of the depleted MORB mantle (DMM). *Earth and Planetary Science Letters* **231**, 53–72.

Wortel, M. J. R. & Spakman, W. (2000). Subduction and slab detachment in the Mediterranean–Carpathian Region. *Science* **290**, 1910–1917.

Yaxley, G. M. & Green, D. H. (1994). Experimental demonstration of refractory carbonate-bearing eclogite and siliceous melt in the subduction regime. *Earth and Planetary Science Letters* **128**, 313–325.

Zou, H. & Zindler, A. (2000). Theoretical studies of $^{238}$U–$^{230}$Th–$^{226}$Ra and $^{235}$U–$^{231}$Pa disequilibria in young lavas produced by mantle melting. *Geochimica et Cosmochimica Acta* **64**, 1809–1817.

Zou, H., Reid, M. R., Liu, Y., Yao, Y., Xu, X. & Fan, Q. (2003). Constraints on the origin of historic potassic basalts from northeast China by U–Th disequilibrium data. *Chemical Geology* **200**, 189–201.

## APPENDIX: ANALYTICAL PROCEDURES

Major elements were determined at the Università degli Studi di Firenze using an integrated method employing X-ray fluorescence (XRF) (Franzini *et al.*, 1972), atomic absorption spectrometry (AAS) (MgO and $Na_2O$) and titration (FeO; Shapiro & Brannock, 1962). Trace element data were determined using XRF (Università degli Studi di Firenze, Italy) and inductively coupled plasma mass spectrometry (ICP-MS) (SGS, Don Mills, Canada).

Sr and Nd isotope compositions were determined at the Università degli Studi di Firenze using a ThermoFinnigan TRITON thermal ionization multi-collector (MC) mass spectrometer. Analyses were performed in dynamic mode, following the procedure described by Avanzinelli *et al.* (2005). Replicates on NIST SRM 987 and La Jolla international reference standards, over the period of the study, yield average values of $^{87}$Sr/$^{86}$Sr = 0·710251 ± 11 ($2\sigma$, $n = 162$) and $^{143}$Nd/$^{144}$Nd = 0·511845 ± 7 ($2\sigma$, $n = 42$). Internal precision (2 SE) is typically ≤10 ppm for both Sr and Nd isotope ratios.

Th and U concentrations, along with $^{230}$Th/$^{232}$Th and $^{234}$U/$^{238}$U ratios, were measured at the Bristol Isotope Group laboratory (University of Bristol, UK) on a ThermoFinnigan Neptune MC-ICPMS system, equipped with a secondary electron multiplier (SEM) located behind an energy filter device (retarding potential quadrupole; RPQ), which produces high abundance sensitivities (usually 30–55 ppb at mass 230 relative to the signal at mass 232). The sample introduction system incorporates a Cetac Aridus nebulizer with a nominal uptake rate of 50 $\mu$l/min and in typical operation yields a $UH^+/U^+$ ratio $<10^{-7}$. Th and U concentrations were determined by isotope dilution using a mixed $^{229}$Th–$^{236}$U spike.

Rock samples were weighed and spiked to obtain $^{229}$Th/$^{230}$Th and $^{232}$Th/$^{229}$Th ratios of ~10–12 and ~15 000, respectively. The samples were digested in a HF–$HNO_3$–$HClO_4$ mixture in Teflon® PFA beakers and subsequently brought into complete solution in HCl. The samples were then loaded in 3N $HNO_3$ onto Teflon® 'shrink-fit' 0·5 ml columns loaded with Eichrom® TRU-Spec resin. The resin was washed with 3N $HNO_3$ and 6N HCl, and Th and U fraction were eventually collected in 0·2N HCl and 0·3N HCl + 0·1N HF, respectively.

The Th and U fractions were measured in separate runs, using a sample bracketing procedure. The Th run consisted of SEM measurement of $^{229}$Th and $^{230}$Th in two different jumps both with simultaneous collection of $^{232}$Th on a Faraday collector: the $^{229}$Th/$^{230}$Th value was then calculated by dividing the two static $^{229}$Th/$^{232}$Th and $^{230}$Th/$^{232}$Th ratios. The same approach was used for the U run: $^{234}$U and $^{236}$U were collected in two different jumps on the SEM, whereas $^{235}$U and $^{238}$U were measured simultaneously on Faraday cups. A bracketing U standard (NBL CRM 112a) was used for both U and Th runs. NBL CRM 112a (hereafter U112a) was measured before and after each U and Th sample. Mass bias and Faraday or SEM yield in the sample were monitored and corrected using the $^{235}$U/$^{238}$U (both measured statically on Faraday cups) and $^{234}$U/$^{238}$U (collected statically on the SEM and Faraday) of the U112a standard, respectively. The samples were run in an analysis sequence that also included a measurement of both Table Mountain Latite (hereafter TML) and additionally Santa Cruz Th-A standard (hereafter SC-Th) in Th runs. After washing, a blank solution was measured before and after each sample or standard, determining 'on-peak backgrounds' on the SEM intensity for each nuclide of interest in the blank solution to allow the effects of 'machine blank' to be corrected. Wash and total procedure blank values were negligible for $^{232}$Th, $^{235}$U, $^{238}$U (<0·04‰ of the measured peak intensities) and slightly higher for $^{230}$Th and $^{234}$U (<0·6‰ and <0·5‰ of the measured peak intensities, respectively).

U–Th analyses were performed, from 2002 to 2004, during the development of the analytical protocols at University of Bristol. Because some of the instrumental procedures have improved subsequent to the data collection, we have reprocessed the data to incorporate later developments. Two SEMs were used over the course of this study, and the initial SEM used was not as fully characterized as those described by Hoffmann *et al.* (2005). Likewise, most of Th measurements were bracketed with a U standard rather than a Th standard, which may influence the accuracy of the yield and mass bias (Pietruszka *et al.*, 2002; Ball *et al.*, 2004; Hoffmann *et al.*, 2005). We have taken an empirical approach to retrospectively correct for some of these effects.

Analyses from March 2002 to June 2003 were measured with a MassCom SEM and bracketed with U112a for both Th and U run as described above. The SEM was tested for non-linearity effects according to the procedure proposed by Richter *et al.* (2001); as this test suggested the occurrence of non-linearity effects only above a limit threshold of ~40 000 c.p.s., all the samples were run keeping $^{234}$U, $^{236}$U, $^{229}$Th and $^{230}$Th intensities below this value; however, this SEM was not characterized for possible low count non-linearity effect (Hoffmann *et al.*, 2005).

To assess the possible presence of this effect, along with the influence of different yield corrections on Th measurements from bracketing with a U or a Th standard, we compared the March 2002–June 2003 data with a few measurements of TML, SC-Th and some replicates of the samples, run in October 2003 in sequences, that employed a well-characterized ETP SEM (Hoffmann *et al.*, 2005) and used an in-house Th standard (i.e. TEDDi: Hoffmann *et al.*, 2005, 2007) as a bracketing standard for Th runs. In these October 2003 sequences the Th data of the unknown standards and samples were corrected using the $^{229}$Th/$^{230}$Th and $^{230}$Th/$^{232}$Th of TEDDi for mass bias and SEM or Faraday yield, respectively; the non-linearity effect was corrected according to equations (6) and (7) of Hoffmann *et al.* (2005).

As found by Hoffmann *et al.* (2005) this ETP SEM was strongly non-linear, with significant non-linearity at all count rates in addition to enhanced non-linearity at higher count rates (e.g. Richter *et al.*, 2001). It is important to highlight that, whereas an underestimation of the non-linearity effect would affect all the counts measured on the SEM and therefore the ($^{230}$Th/$^{238}$U) activity ratios of the unknown samples, the effect of an inaccurate yield correction for the Th run would result in inaccurate $^{230}$Th/$^{232}$Th, but would not affect the ($^{230}$Th/$^{238}$U) activity ratios, because ($^{230}$Th) activity was derived by the dynamic SEM/SEM $^{229}$Th/$^{230}$Th ratio, which does not require a Faraday or SEM correction. For this reason is it possible to use the ($^{230}$Th/$^{238}$U) of the TML measured with the incompletely characterized MassCom SEM as a test for any possible low count rate non-linearity. The resulting ($^{230}$Th/$^{238}$U) activity ratios of the TML standard measurements were $0{\cdot}998 \pm 3$ ($2\sigma$, $n = 7$) for the March 2002–June 2003 sequences and $1{\cdot}002 \pm 4$ ($2\sigma$, $n = 4$) for the October 2003 sequences. These data suggest a negligibly low count non-linearity effect for the MassCom SEM and therefore no further non-linearity correction was applied to the data measured in the March 2002–June 2003 sequences; this finding is also consistent with the minor non-linearity effect at low count rates measured for the MassCom SEM currently in use at University of Bristol (10 times lower than the ETP SEM used for the October 2003 sequences; Hoffmann *et al.*, 2007).

The TML standards measured in the March 2002–June 2003 sequences (i.e. U112a bracketed) yielded lower $^{230}$Th/$^{232}$Th values than those for the October 2003 sequences (i.e. TEDDi bracketed) and were strongly variable, depending on the SEM operating condition. To take into account these yield-related differences, the $^{230}$Th/$^{232}$Th ratio of TML ($5{\cdot}782 \pm 23 \times 10^{-6}$, $2\sigma$, $n = 4$) was used to normalize the Faraday or SEM yield of the U112a bracketed sequences (March 2002–June 2003). SC-Th was used as a test of the accuracy of the correction.

Using this procedure for the U112a bracketed SC-Th we obtained $^{230}Th/^{232}Th = (5{\cdot}801 \pm 29) \times 10^{-6}$ ($2\sigma$, $n = 8$), identical within error to the value obtained in the TEDDi bracketed runs [$^{230}Th/^{232}Th = (5{\cdot}792 \pm 4) \times 10^{-6}$, $2\sigma$, $n = 3$].

Overall, the reproducibility of our Th measurements can be determined from the measurements of TML for the ($^{230}Th/^{238}U$) activity ratios ($0{\cdot}999 \pm 5$, $2\sigma$, $n = 10$) and from SC-Th for the $^{230}Th/^{232}Th$ [$(5{\cdot}802 \pm 32) \times 10^{-6}$, $2\sigma$, $n = 11$]. The accuracy and reproducibility of the U analyses were also tested using the ($^{234}U/^{238}U$) activity ratio of TML, which has a mean value of $1{\cdot}000 \pm 6$ ($2\sigma$, $n = 10$).

The internal errors of the U and Th analyses need to incorporate the combined effects of several corrections required in the sample bracketing procedure for overall error. We adopted a Monte Carlo approach to propagate the error on the bracketing standards measurements and on their absolute number (i.e. the error propagation in the mass bias and yield correction), and the error on the blank solution measurements, to generate an overall uncertainty. A further error propagation has been applied for the age correction, including the reported errors for the age determination (Table 1). On average, the internal propagated errors before age correction are ~0·4% for ($^{230}Th/^{238}U$), ~0·5% for both ($^{230}Th/^{232}Th$) and ($^{238}U/^{232}Th$), and ~0·3% for ($^{234}U/^{238}U$). All the absolute propagated errors for both corrected and uncorrected ratios are reported in Table 3.